

# Structural and $P$ – $T$ Evolution of a Major Cross Fold in the Central Zone of the Limpopo High-Grade Terrain, South Africa

D. D. VAN REENEN<sup>1\*</sup>, L. L. PERCHUK<sup>2,3</sup>, C. A. SMIT<sup>1</sup>,  
D. A. VARLAMOV<sup>3</sup>, R. BSHOFF<sup>1</sup>, J. M. HUIZENGA<sup>1</sup> AND  
T. V. GERYA<sup>3,4</sup>

<sup>1</sup>DEPARTMENT OF GEOLOGY, RAND AFRIKAANS UNIVERSITY, P.O. BOX 524, AUCKLAND PARK, 2006, JOHANNESBURG, SOUTH AFRICA

<sup>2</sup>DEPARTMENT OF PETROLOGY, GEOLOGICAL FACULTY, MOSCOW STATE UNIVERSITY, VOROBIEVY GORY, MOSCOW, 119899 RUSSIA

<sup>3</sup>INSTITUTE OF EXPERIMENTAL MINERALOGY, RUSSIAN ACADEMY OF SCIENCES, CHERNOGOLOVKA, MOSCOW DISTRICT, 142432, RUSSIA

<sup>4</sup>INSTITUT FÜR GEOLOGIE, MINERALOGIE UND GEOPHYSIK, FAKULTÄT FÜR GEOWISSENSCHAFTEN, RUHR-UNIVERSITÄT-BOCHUM, 44780 BOCHUM, GERMANY

RECEIVED NOVEMBER 15, 2002; ACCEPTED FEBRUARY 26, 2004

*The Central Zone (CZ) of the Limpopo Complex of southern Africa is characterized by a complex deformational pattern dominated by two types of fold geometries: large sheath folds and cross folds. The sheath folds are steeply SSW-plunging closed structures whereas the cross folds are north–south-oriented with near-horizontal fold axes. In the area south of Messina this complexly folded terrain grades continuously towards the south into a crustal-scale ENE–WSW-trending ductile shear zone with moderate dip towards the WSW. All sheath folds document consistent top-to-the-NE thrust movement of high-grade material. The timing of this shear deformational event ( $D_2$ ) and thus of the gneissic fabric ( $S_2$ ) is constrained (at  $\sim 2.6$  Ga) by the syntectonic emplacement throughout the CZ of precursors to quartzo-feldspathic gneisses (Singelele-type gneisses). Cross folds deform the  $S_2$  fabric and are characterized by a near-vertical axial planar cleavage ( $S_3$ ). Recent single-phase Pb–Pb dating of garnet from a metapelitic gneiss with an  $S_3$  fabric from one of the largest cross folds in the CZ constrains the timing of the deformational ( $D_3$ ) and metamorphic ( $M_3$ ) event at  $\sim 2.0$  Ga. Mineral chemistry for metapelites from this cross fold shows a single peak on an  $N_{Mg}$  histogram for garnet reflecting a single phase of mineral growth. Metapelites from this cross fold also preserve evidence for only one well-developed reaction texture,  $Grt + Sil + Qtz \rightarrow Crd$ . This reaction is accompanied by the simultaneously operating reaction  $Grt + Fsp + H_2O = Bt + Sil + Qtz$ . Both*

*these divariant reactions belong to the univariant KFMASH equilibrium  $Crd + Grt + Fsp + H_2O \rightarrow Bt + Sil + Qtz$ . The progress of the two divariant retrograde reactions leads to the consumption of Grt and Fsp: K-feldspar ( $Or_{94-100}$ ) never occurs with both cordierite and garnet. Microprobe profiling coupled with calculated isopleths for Bt, Grt and Crd in divariant equilibria define a decompression-cooling P–T path that reflects a single ( $M_3$ ) high-grade metamorphic event during the evolution of the cross fold. This decompression-cooling P–T path traverses from  $780^\circ\text{C}$ , 5–7 kbar to  $600^\circ\text{C}$ , 3–3 kbar.*

KEY WORDS: deformation; granulites; Limpopo Complex; geothermobarometry; mineral equilibrium; mineral thermodynamics; P–T path

## INTRODUCTION

The 700 km  $\times$  250 km Limpopo Complex of Southern Africa is a unique field laboratory for studying fundamental problems of the formation and exhumation of granulite-facies terrains located between Precambrian cratons (e.g. Van Reenen *et al.*, 1992). Mason (1973) was the first to subdivide the complex into three tectonic units: the Late Archaean Southern (SMZ) and Northern

\*Corresponding author. Fax: +27-11-4892309. E-mail: dddv@na.rau.ac.za

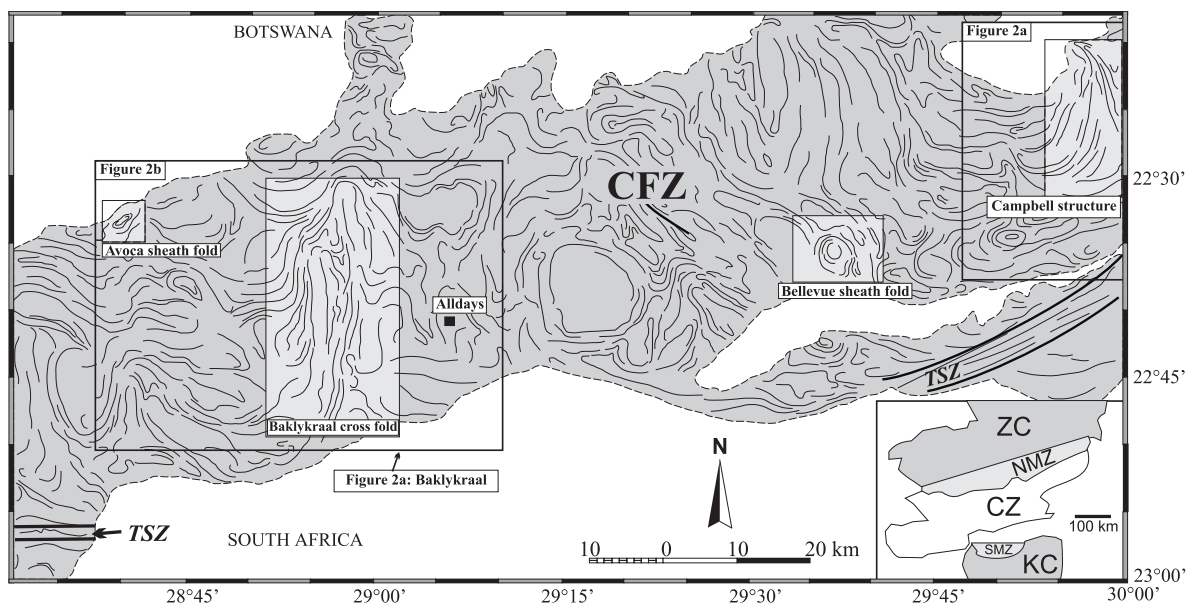


**Fig. 1.** Structural pattern of the Central Zone of the Limpopo Complex in South Africa, modified after the published 1:250 000 geological map (2228 Alldays). The Tshipise Straightening Zone (TSZ) in the south and the Cross Folded Zone (CFZ) in the north are shown. Important sheath folds (Avoca and Bellevue) and cross folds (Baklykraal and Campbell) are highlighted and the location of Fig. 2a and b is shown. Inset shows the Limpopo Complex (CZ, SMZ, and NMZ) located between the Zimbabwe craton (ZC) and Kaapvaal craton (KVC).

(NMZ) Marginal Zones (e.g. Mkweli *et al.*, 1995; Kreissig *et al.*, 2001) and a Central Zone (CZ) located between the SMZ and NMZ. Most workers agree that the two marginal zones were exhumed and emplaced in the Late Archaean. The age of the formation and  $P$ - $T$  history of the CZ is still being debated.

Barton *et al.* (1994), Kamber *et al.* (1995), Holzer *et al.* (1998), and Schaller *et al.* (1999) published evidence based on single-phase dating of metamorphic minerals for three distinct events in the CZ: (1) a Mid-Archaean ( $\sim 3.2$  Ga) event mainly reflected by magmatic activity with relic traces of an early deformational and metamorphic event (here termed  $D_1/M_1$ ); (2) a Late Archaean ( $\sim 2.57$ – $2.65$  Ga) low-pressure ‘anticlockwise’ granulite-facies event (here termed  $D_2/M_2$ ) associated with granitic/charnockitic magmatism that resulted from vertical crustal growth of the Zimbabwe Craton; (3) a Palaeoproterozoic ( $\sim 2.05$ – $1.95$  Ga) HP-HT clockwise granulite-facies event (here termed  $D_3/M_3$ ) caused by the collision of the Zimbabwe and Kaapvaal cratons. In this interpretation the complex deformational pattern of the CZ mainly reflects the Palaeoproterozoic event ( $D_3/M_3$ ) that obliterated most of the evidence for the two Archaean events.

Hofmann *et al.* (1998) and Kröner *et al.* (1998, 1999), on the basis of single-zircon dating of syntectonic granitic magmatism, also documented evidence for three distinct events, but with a different emphasis on the relative significance of the last two events. Those workers concluded that the late Archaean  $D_2/M_2$  event represents the major fabric-forming episode in the CZ, and other deformation events are subordinate: the  $\sim 2.0$  Ga

Palaeoproterozoic event is thus considered to be mainly a high-grade static metamorphic event (e.g. Hofmann *et al.*, 1998; McCourt & Armstrong, 1998), suggesting that the complex deformational pattern of the CZ mainly reflects the late Archaean  $D_2/M_2$  event.

Published data can therefore be interpreted to suggest that the deformational pattern of the CZ, dominated by two major folded structures—cross folds and sheath folds (Figs 1 and 2)—reflects a major high-grade deformational event, either in the Late Archaean (Hofmann *et al.*, 1998; Kröner *et al.*, 1998, 1999) or in the Palaeoproterozoic (Holzer *et al.*, 1998; Schaller *et al.*, 1999). New age data (Boshoff, 2004), however, are not in accordance with the formation of the CFZ as the result of a single geodynamic event. These new data constrain the age of (1) a major sheath fold (the Avoca sheath fold), based on zircon sensitive high-resolution ion microprobe (SHRIMP) data from syn- to late tectonic precursors to the Singelele-type gneisses, to  $\sim 2.57$  Ga, and (2) a major cross fold (the Baklykraal fold), based on single-phase dating of garnet from metapelitic gneisses, to  $\sim 2.0$  Ga.

The thermodynamic ( $P$ - $T$ -fluid) history of the CZ is also still the subject of debate. Several studies (e.g. Horrocks, 1983; Harris & Holland, 1984; Droop, 1989; Van Reenen *et al.*, 1990; Hisada & Miyano, 1996) proposed essentially isothermal decompression (ITD) of the high-grade rocks, which implies an extremely high speed of exhumation of the CZ: the velocity of upward movement should be much higher than the rate of heat loss. In addition, none of these studies integrated detailed structural data with the proposed  $P$ - $T$  trajectories. In contrast,

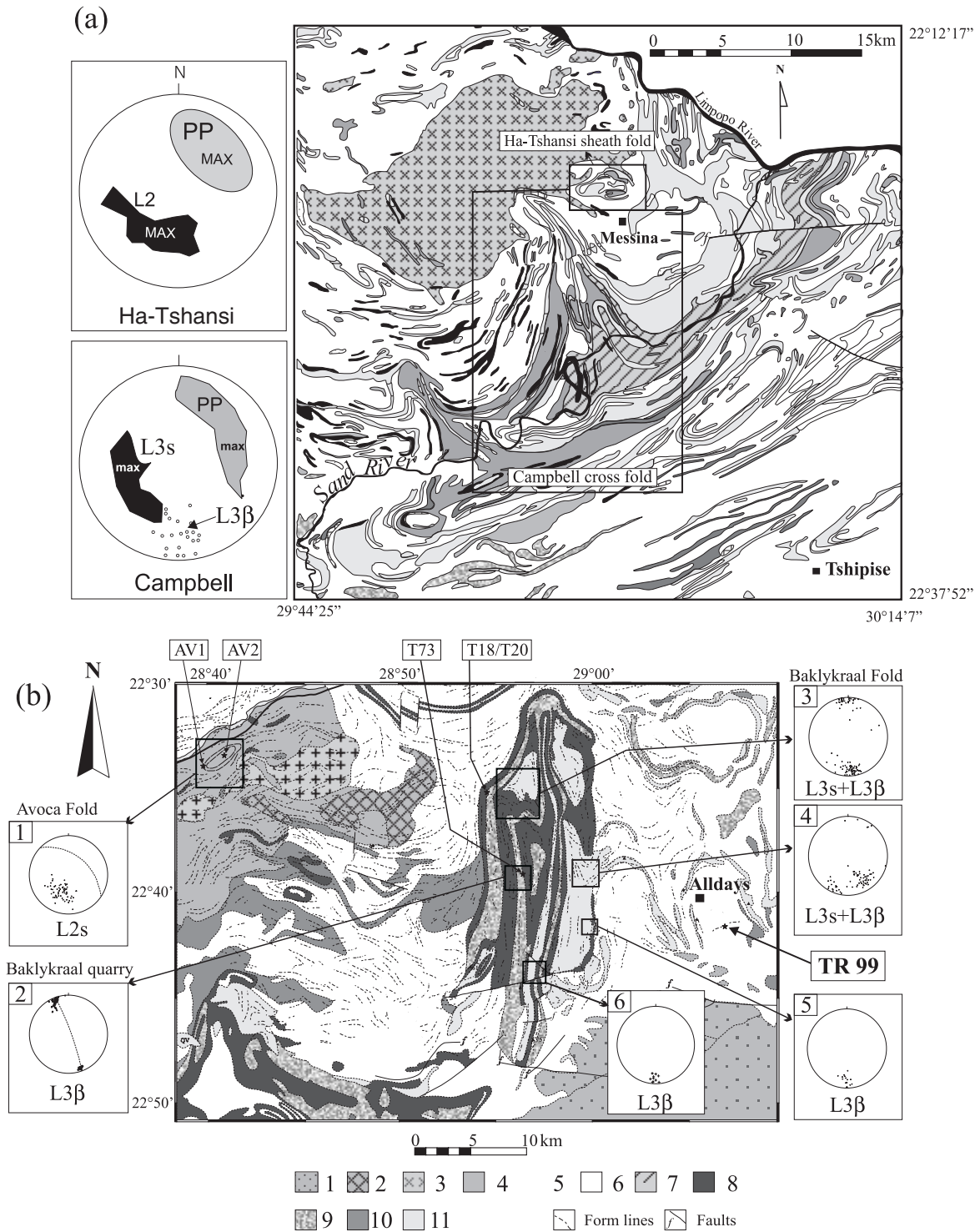


**Fig. 2.** (a) Geological map of the area surrounding Messina showing outcrops of the Sand River Gneiss SE and south of Messina, a major sheath fold (Ha-Tshansi), the Campbell cross fold, and the Bulai pluton. (b) Geological map of the Baklykraal area showing the Baklykraal cross fold and the Avoca sheath fold. Lower hemisphere stereographic projections of structural data show poles to planes (PP) and linear elements including kinematic stretching ( $L_s$ ) and geometric lineations ( $L_\beta$ ). 1, Karoo sediments; 2, syenite pluton; 3, Bulai pluton; 4, Singelele quartzo-feldspathic gneisses; 5, Alldays porphyroblastic gneisses; 6, Alldays grey migmatitic gneisses; 7, Sand River Gneiss; 8, anorthositic and leuco-gabbroic gneisses (Messina Suite); Beit Bridge Complex: 9, marbles and calc-silicates; 10, amphibolites with bands of metapelites, 11, massive quartzites. TR99, Alldays porphyroblastic gneiss with a Pb–Pb age of  $2650 \pm 21$  Ma (Kröner *et al.*, 1999); AV1 and AV2 represent Singelele gneiss (Pb–Pb age of  $2651 \pm 8$  Ma) from the rim of the Avoca sheath fold and Avoca granite, respectively (Pb–Pb age of  $2570 \pm 22$  Ma) (Boshoff, 2004).

structural, metamorphic and physicochemical studies of major structures in the SMZ (Smit *et al.*, 2001), supported by limited data from the CZ by Perchuk *et al.* (1996, 2000), have demonstrated that the decompressional-cooling (DC) of the high-grade rocks of these two zones suggests a broad match between the rate of exhumation and associated heat loss (Gerya *et al.*, 2000). These results are consistent with the concept (Perchuk, 1989) of the gravitational redistribution of the initial cratonic rocks that resulted in the formation of the entire Limpopo high-grade terrain at  $\sim 2.65$  Ga.

The aim of this paper is twofold: (1) to demonstrate the coherent structural and metamorphic evolution of one of the largest cross folds in the CZ (Baklykraal fold, Figs 1 and 2b); (2) to correctly derive the  $P$ - $T$  path for this giant structure.

We use the following mineral abbreviations and thermodynamic symbols.

*Mineral abbreviations used.* Act, actinolite; And, andalusite; Ann, annite; Bt, biotite; Cal, calcite; Crd, cordierite; Di, diopside; East, eastonite; Fsp, feldspar; Grt, garnet; Kfs, K-feldspar; Ky, kyanite; Oam, orthoamphibole; Opx, orthopyroxene; Phl, phlogopite; Pl, plagioclase; Prp, pyrope; Qtz, quartz; Rut, rutile; San, sanidine; Sil, sillimanite; Spl, spinel.

*Thermodynamic symbols used.*  $T$ , temperature (K or  $^{\circ}\text{C}$ );  $P$ , pressure (bar or kbar);  $\Delta G^{\circ}$ , the change of standard Gibbs free energies in a reaction;  $R = 1.987$  cal (1 cal = 4.186 J) is the gas constant;  $X_i$ , mole fraction of component  $i$  in a given phase;  $X_{\text{Mg}} = \text{Mg}/(\text{Mg} + \text{Fe})$ ;  $N_i = 100X_i$ ;  $N_{\text{Mg}}$ , Mg-number;  $a_{\text{Crd}}$ , activity of dry cordierite in the system  $\text{Crd}_{\text{dry}} - \text{Crd}_{\text{H}_2\text{O}-\text{CO}_2}$ ,  $\mu_{\text{H}_2\text{O}}^{\text{fluid}} = \mu_{\text{H}_2\text{O}}^{\circ} + RT \ln a_{\text{H}_2\text{O}}^{\text{fluid}}$ ;  $\mu_{\text{H}_2\text{O}}^{\circ} = RT \ln f_{\text{H}_2\text{O}}^{\circ}$ , chemical potential of pure water as function of  $P$  and  $T$ ;  $f_{\text{H}_2\text{O}}^{\circ}$ , water fugacity;  $a_{\text{H}_2\text{O}}^{\text{fluid}} = \gamma_{\text{H}_2\text{O}}^{\text{fluid}} X_{\text{H}_2\text{O}}^{\text{fluid}}$ ,  $\text{H}_2\text{O}$  activity in the fluid phase where  $\gamma_{\text{H}_2\text{O}}^{\text{fluid}}$  is  $\text{H}_2\text{O}$  activity coefficient in a fluid phase;  $G_i^{\text{m}} = RT \ln a_i$ , partial molar mixing Gibbs free energy for component  $i$  of a solid solution;  $G_i^{\text{c}}$ , partial molar excess Gibbs free energy for component  $i$  in a solid solution;  $G^{\text{c}}$ , integral molar excess Gibbs free energy of a solid solution;  $W_{ij}$ , the Margules interaction parameter (cal/mol).

## GEOLOGICAL FRAMEWORK OF THE CENTRAL ZONE

The Limpopo Complex comprises, as mentioned above, three crustal domains (Mason, 1973): the CZ, SMZ and NMZ. The latter two domains are separated from the adjacent cratons by  $\sim 2.6$  Ga (Kreissig *et al.*, 2001) inward-dipping crustal-scale ductile dip-slip shear zones along which the granulite-facies rocks have been thrust onto the adjacent cratons (Van Reenen *et al.*, 1987, 1992; Roering *et al.*, 1992; Smit & Van Reenen, 1997): the Hout River Shear Zone in the south, and the North Marginal Thrust Zone in the north (e.g. Mkweli *et al.*, 1995).

The high-grade rocks from the two marginal zones have lithological and geochemical similarities to lower-grade rocks from the adjacent granite-greenstone cratons (Van Reenen & Smit, 1996; Kreissig *et al.*, 2000), suggesting their derivation through metamorphism of the latter rocks under lower-crustal conditions.

The CZ is bounded by crustal-scale inward-dipping  $\sim 2.0$  Ga strike-slip mylonitic/cataclastic shear zones, the Palala Shear Zone in the south, and the Triangle Shear Zone in the north (e.g. McCourt & Vearncombe, 1992; Kamber *et al.*, 1995; Schaller *et al.*, 1999). The CZ consists of a wide range of lithologies, including high-grade metamorphic platform sediments (the Beit Bridge Complex), intruded at  $\sim 3.3$  Ga by granitoids, named the Sand River Gneiss (SRG) and by mafic-ultramafic rocks of the Messina Suite (MS), related to the Mid-Archaean ( $D_1/M_1$ ) event (e.g. Kröner *et al.*, 1999). Subsequently (at  $\sim 2.6$  Ga) granitic intrusions of various ages, including the precursors to the Alldays- and Singelele Gneisses and the Bulai pluton, were emplaced in the Beit Bridge Complex, SRG and MS (e.g. Van Reenen *et al.*, 1990; Hofmann *et al.*, 1998; Kröner *et al.*, 1998, 1999). Syntectonic magmatism (related to the Alldays and Singelele Gneisses) occurred between  $\sim 2.67$  and  $\sim 2.57$  Ga and accurately dates the  $D_2/M_2$  Late Archaean event (e.g. Kröner *et al.*, 1999). The Bulai pluton, on the other hand, was emplaced into high-grade ductilely deformed rocks of the Beit Bridge Complex in the area west of Messina at 2.57 Ga (Barton *et al.*, 1994) (Fig. 2a), and shows little evidence of the  $D_2$  deformation event (Mccourt & Armstrong, 1998).

The  $D_2/M_2$  event is thus related to an  $\sim 100$  Myr period of extensive granitic magmatism that occurs throughout the Limpopo Complex (Kröner *et al.*, 1999). Clear evidence for a deformational event ( $D_3$ ) that post-dates  $D_2$  in the area SE and east of Messina, according to Hoffman *et al.* (1998) and Kröner *et al.* (1998, 1999), is expressed by various sets of shear zones. Similar shear zones are also developed in the Bulai pluton (Watkeys, 1983), and various undeformed granitic patches and pegmatite veins are dated at  $\sim 2.0$  Ga (e.g. Holzer *et al.*, 1998; Kröner *et al.*, 1999).

The complex regional deformation pattern that characterizes the entire CZ (Fig. 1) comprises two major structural domains, namely a high-grade ENE-WSW-directed 'Straightening Zone' in the south, and the complex folded area north of the Straightening Zone referred to as the 'Cross Folded Zone' (CFZ) (Fig. 1) (Söhnge, 1946; Bahneman, 1972; Watkeys, 1983). The Tshipise Straightening Zone is characterized by a monotonous ENE-WSW-trending foliation pattern that dips steeply towards the SSE. Fold axes and lineations dip moderately towards the WSW (Fripp, 1983). Two major folded structures are recognized in the CFZ: (1) cross folds, i.e. a regional spread of large NNW-SSE-trending folds with

near-horizontal fold axes perpendicular to the regional strike of the CZ (e.g. Söhnge, 1946; Bahneman, 1972; Pienaar, 1985; Pretorius, 1986; Feldtmann *et al.*, 1995; Feldtmann, 1996); (2) sheath folds characterized by moderately WSW-plunging central fold axes (Roering *et al.*, 1992). The best examples of sheath folds in the CZ in South Africa include the Avoca fold developed in quartzo-feldspathic gneisses (Singelele Gneiss) in the Baklykraal area west of Alldays (Fig. 2b, stereonet 1), and the Bellevue (Fig. 1) and Ha-Tshansi (Fig. 2a) folds developed in rocks of the Beit Bridge Complex near Messina. Two major cross folds are represented by the Baklykraal (Fig. 2b) and Campbell (Fig. 2a) folds.

All sheath folds in the CZ demonstrate identical fold geometries with central fold axes that show consistent top-to-the-NE movement (e.g. Fig. 2a and b). The Avoca sheath fold (Fig. 2b) is developed in Singelele-type gneisses about 20 km WNW of the Baklykraal cross fold and is an important time marker for the development of sheath folds in the CZ, and thus of the  $D_2/M_2$  event. Boshoff (2004) have obtained sensitive high-resolution ion microprobe (SHRIMP) Pb–Pb zircon ages of  $2651 \pm 8$  Ma from gneisses in the rim of the structure. These gneisses preserve a strong  $S_2$  shear fabric and a single population of mineral stretching lineations ( $L_2$ , Fig. 2b, stereonet 1) that define a steeply SW-oriented central fold axis. These penetratively deformed gneisses grade continuously into an unfoliated, but strongly lineated variety of the same rock (the Avoca granite) in the core of the oval-shaped structure. Mineral stretching lineations in the Avoca granite (dated at  $2570 \pm 22$  Ma, Boshoff, 2004) are also developed parallel to the central axis of the fold. The Avoca sheath fold therefore constrains the timing of the  $D_2/M_2$  tectonometamorphic event within a relatively narrow time period in the Late Archaean.

### Structural evolution of the Baklykraal cross fold

The 40 km  $\times$  80 km Baklykraal cross fold (Fig. 2b) offers an ideal opportunity to study the structural and metamorphic evolution of cross folds in the CZ as well as the timing of this important event based on single-phase dating of garnet in metapelitic gneisses (Boshoff, 2004). The Baklykraal cross fold is an ENE-trending synformal structure with a near-horizontal fold axis developed in gneissic rocks of the Beit Bridge Complex. These include marble, calc-silicates, mafic gneisses, quartzites, garnet–biotite gneisses and minor metapelitic gneisses. Two well-developed fabrics ( $S_2$ ,  $S_3$ ) are present within the rocks forming the Baklykraal fold. The  $S_2$  gneissic fabric that defines the form of this structure (Fig. 2b, stereonets 2–6) in outcrop is similar to the  $S_2$  gneissic fabric of the sheath folds. However, in outcrop  $S_2$  is often enhanced by trails of small garnet grains or by elongated garnet grains that are oriented parallel to the fold axis. This  $S_2$  gneissic

fabric in the nose portion of the fold is cut by a near-vertical north–south-oriented axial planar  $S_3$  cleavage (Fig. 2b, stereonets 2–6). This relationship can be interpreted to suggest that the  $S_2$  fabric preserved in the Avoca and similar sheath folds in the CZ was reworked during a subsequent geological event that resulted in the formation of the cross folds. The reworked  $S_2$  fabric is thus referred to as  $S_3$ .

Two populations of linear elements are also displayed. Feldtmann (1996) recorded a population of linear elements (boudinaged calc-silicates, cigar-shaped pegmatite boudins, quartz rods, minor fold axis, etc.) from the Baklykraal quarry (Fig. 2b, stereonet 2) developed in marble and calc-silicates near the centre of the fold. These elements demonstrate a consistent linear direction that plunges at 5–12° in a general north–south direction, defining the  $\beta$ -fold axis of the synformal structure and are referred to as  $L_{3\beta}$ . A second population of moderately SW-plunging mineral stretching lineations ( $L_{3s}$ ) are also developed in metaquartzite (Fig. 2b, stereonet projections 3 and 4), suggesting movement of material to the NE along planes that developed parallel to the original bedding planes, mainly within the limbs of the fold.

The presence of two fabric-forming events ( $D_2$ ,  $D_3$ ) in the Baklykraal cross fold is also supported by recent single-phase dating of garnet (Boshoff, 2004) from a metapelitic gneiss with an  $S_3$  fabric (Fig. 2b, sample T73). The results of this study suggest that the garnet in sample T73 grew during a high-grade metamorphic ( $M_3$ ) and deformational ( $D_3$ ) event at  $\sim 2.0$  Ga. The asymmetric Campbell cross fold (Figs 1 and 2a) near Messina displays a similar structural geometry and is, therefore, considered to have developed at the same time.

In the following sections we decipher the metamorphic evolution of metapelitic gneisses from the Baklykraal cross fold.

## METAMORPHISM

### Petrography

The main purpose of this section is (1) to characterize the mineral assemblages and their compositions in the rocks from the Baklykraal cross-fold, and (2) to show the relationships between the minerals in the various rock types. This allows us to create the basis for a detailed thermobarometric study.

With the exception of massive recrystallized almost pure quartzite all rock types from the Baklykraal structure are in outcrop characterized by a thinly banded gneissic layering often enhanced by strongly attenuated leucocratic zones. However, different rocks from this structure show different degrees of deformation, varying from unfoliated (e.g. J4, Table 1) to highly foliated (T73, T20, T53, Table 1). This observation is very common for high-grade gneisses over the entire Limpopo Complex

Table 1: Selected mineral assemblages of the rocks from the Baklykraal structure

Sample no.	Rock type	Mineral assemblage
T18	Metapelite	Bt + Grt + Qtz + Kfs + Pl + Sil + Rt + Zrc + partly altered Crd
T20	Metapelite	Bt + Grt + Qtz + Pl + Rt + Zrc + partly altered Crd
T73	Metapelite	Bt + Grt + Qtz + Crd + Sil + Kfs + Pl + Ms + Rt + Zrc
T57	Gneiss	Bt + Grt + Qtz + Kfs + Pl + Rt + Zrc
T76	Gneiss	Bt + Grt + Qtz + Kfs + Pl + Sil + Rt + Zrc
T53	Gneiss	Bt + Qtz + Sil + Kfs + Pl + a few Grt
J4	Gneiss	Bt + Grt + Qtz + Sil + Mic + Pl
J123	Gneiss	Bt + Grt + Qtz + Kfs + Pl + Sil + Rt + Zrc
T26	Orthoamphibole rock	Oam + Opx + Qtz + Pl
T19	Orthoamphibole rock	Oam + Grt + Qtz + Pl + (Bt + Sil occur in 10–20 µm thin shear zones)

(e.g. Van Reenen *et al.*, 1990; Smit & Van Reenen, 1997; Smit *et al.*, 2001). Recrystallized quartzite contains more than 90 modal % quartz with minor K-feldspar, albitic plagioclase, Fe-rich spinel, biotite, and accessory minerals such as zircon, apatite, sphene, and ilmenite. Garnet-bearing grey gneisses include three major varieties: (1) orthoamphibole–garnet–quartz–plagioclase gneisses; (2) biotite–garnet–plagioclase–quartz–sillimanite gneisses; (3) cordierite-bearing metapelitic gneisses (see Table 1) that are the major focus of this study. Up to several metres thick calc-silicate and marble units are intercalated with mafic and pelitic gneisses.

Mg-rich orthoamphibole-bearing rocks (Pienaar, 1986) do not show any reaction textures. All samples studied show either a weak foliation or no foliation at all (e.g. J4 in Table 1). In addition to orthoamphibole the rocks always contain orthopyroxene, plagioclase and quartz. In some varieties of this rock type high-aluminium orthoamphibole coexists with cordierite and orthopyroxene. Orthoamphibole-bearing rocks are locally characterized by the presence of micro shear zones composed of fine-grained mylonitic material that includes the assemblage biotite–sillimanite–quartz.

Biotite–garnet gneisses contain sillimanite, quartz, plagioclase and K-feldspar. Some gneisses (e.g. T53, Table 1) are poor in garnet but rich in sillimanite, whereas others show the opposite relation. Despite the fact that the gneisses are migmatitic there is no evidence for the reaction microtexture  $Bt + Sil + Qtz \rightarrow Crd + Grt + Kfs + melt$  that would indicate the fluid-absent melting of biotite. The gneisses also contain thin, <150–200 µm thick, micro shear zones composed of intergrowths of sillimanite and quartz. In comparison with the matrix of this rock, these micro shear zones are poor in potassium-bearing minerals such as K-feldspar and biotite, which are concentrated along the margins of the zones.

Marbles and calc-silicate rocks are well exposed in the Baklykraal quarry in three dimensions. The following

three petrographic groups (see also Feldtmann, 1996) of consistent mineral compositions occur among marbles (all minerals are given in modal %): (1) calcite marble with rare phlogopite and diopside; (2) phlogopite marble (Cal 70–80, Phl 5–15, Di 3–5, Qtz 3 and secondary actinolite after Di); (3) diopside–phlogopite marble (Cal 85, Di 3–5, Phl 3–1, and also scapolite, quartz, K-feldspar, dolomite and tourmaline). The calc-silicate rocks are severely boudinaged, a feature that is well exposed in both the vertical and horizontal plane in the quarry. The compositional banding is characterized by alternating layers of fine-grained Di–Phl- and Qtz–Kfs–Cal-rich zones on millimetre to centimetre scale. The most prominent feature of the rock is the strong orientation of phlogopite parallel to the banding. Both the marbles and calc-silicates contain small (centimetre size) boudins composed of quartzite, metapelite and pegmatite. The long axes of all kinematic elements are oriented parallel to the fold axis of the cross fold (Fig. 2b, stereonet projection 2).

Metapelites occur as lenses, boudins and thin layers (up to a few metres thick) in biotite–garnet and mafic gneisses, and marble, as well as enclaves in quartzite. Typical mineral assemblages and microtextures of metapelites are shown in Table 1 (samples T18, T20, T73) and Figs 3–6, respectively. In outcrop metapelites display leucosomes, migmatitic patches and narrow cross-cutting granitic veins. The well-developed  $S_3$  gneissic foliation is often enhanced by the parallel orientation of biotite, sillimanite and by the presence of very narrow trains of small  $D_3$  garnet grains or elongated  $D_3$  garnet porphyroblasts that are oriented parallel to the fold axis ( $L_{3\beta}$ ) of the cross fold (see Fig. 4e and f). Small, up to 1.5 cm, Qtz-rich lenses also occur along the foliation. The lenses are coated by biotite and cordierite, and, in places, contain almost euhedral Grt porphyroblasts. Rare Bt–Sil–Qtz micro shear zones always follow the foliation (see Fig. 5d). The leucocratic material of metapelites does not preserve evidence for the fluid-absent melting reaction

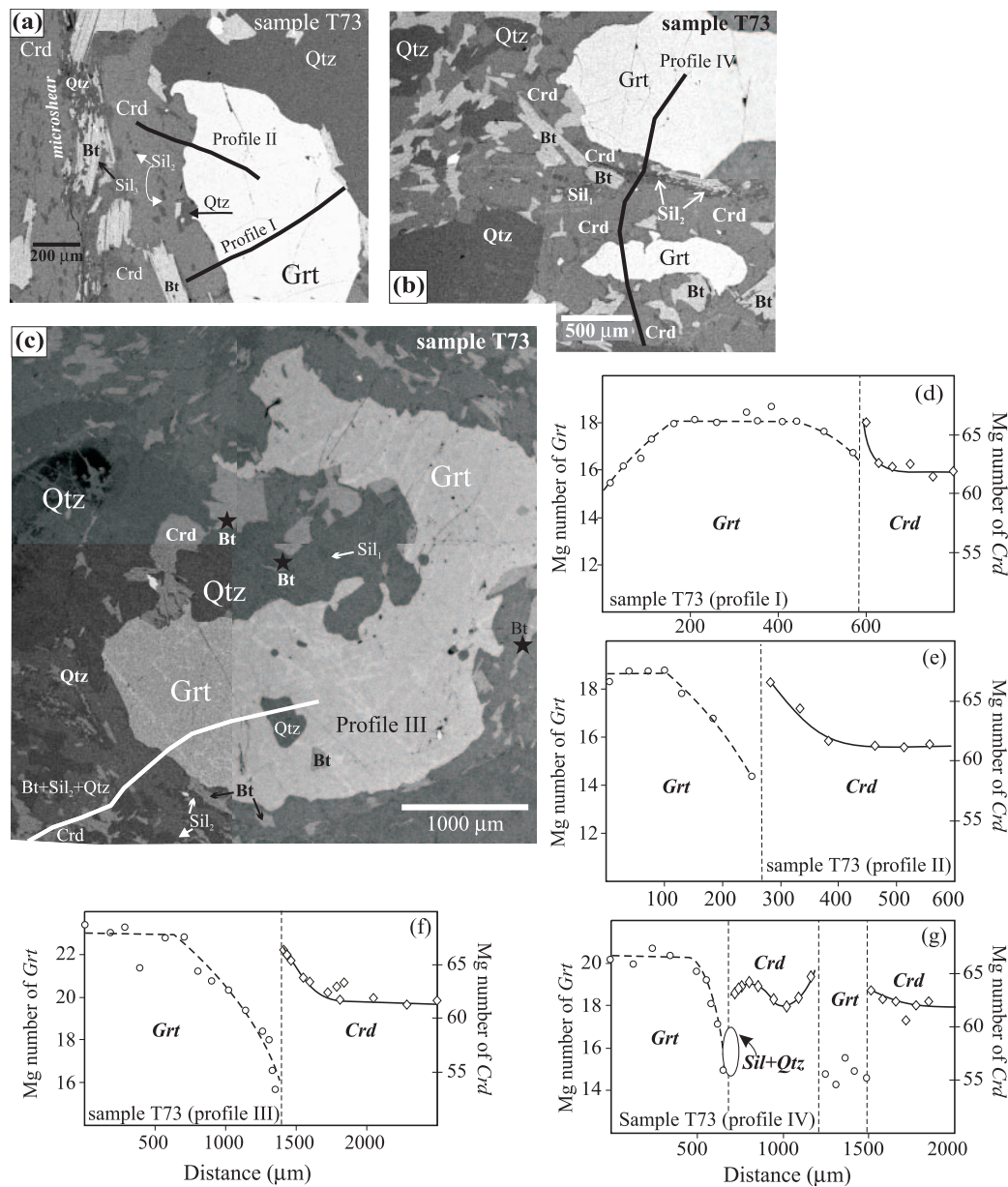


**Fig. 3.** (a–c) BSI of reaction textures developed in sample T73 from the Baklykraal structure illustrating the texture that resulted from reaction (1). Continuous black and white lines in the BSI are microprobe profiles I–IV. (c) shows the locations of biotite (black stars) in contact with sillimanite, quartz, and K-feldspar. Selected analyses of Fe–Mg minerals are listed in Tables 2 and A1. (d)–(g) show results of microprobe analyses along the related profiles. Typical diffusional shapes of the profiles are not seen in the rims of garnets. Compositions of cordierite and garnet in the central portions of profiles in (d)–(g) are approximated by flat lines because of small and non-systematic changes in  $N_{Mg}$  of the minerals. These cores presumably reflect the peak metamorphic compositions.

$Bt + Sil + Qtz \rightarrow Crd + Grt + Kfs + melt$ . This suggests that at the peak of metamorphic conditions the metapelites did not experience partial melting. However, to avoid possible effects related to late migmatitic events, only leucosome-free pelitic samples were used in our studies.

Porphyroblastic grains of quartz and garnet occur in a granoblastic matrix composed of biotite, feldspars, quartz

and sillimanite. Apart from the matrix sillimanite ( $Sil_1$ ) a second generation,  $Sil_2$ , occurs with  $Qtz$  and  $Bt$  as a part of the reaction textures developed around the garnet porphyroblasts. In addition, sillimanite ( $Sil_3$ ) together with  $Qtz$  forms up to 150–200  $\mu m$  thin shear zones showing ambiguous relationships with the reaction textures (see Figs 3a and 5a). Cordierite occurs in slightly altered well-developed corona textures replacing garnet (Fig. 4a),

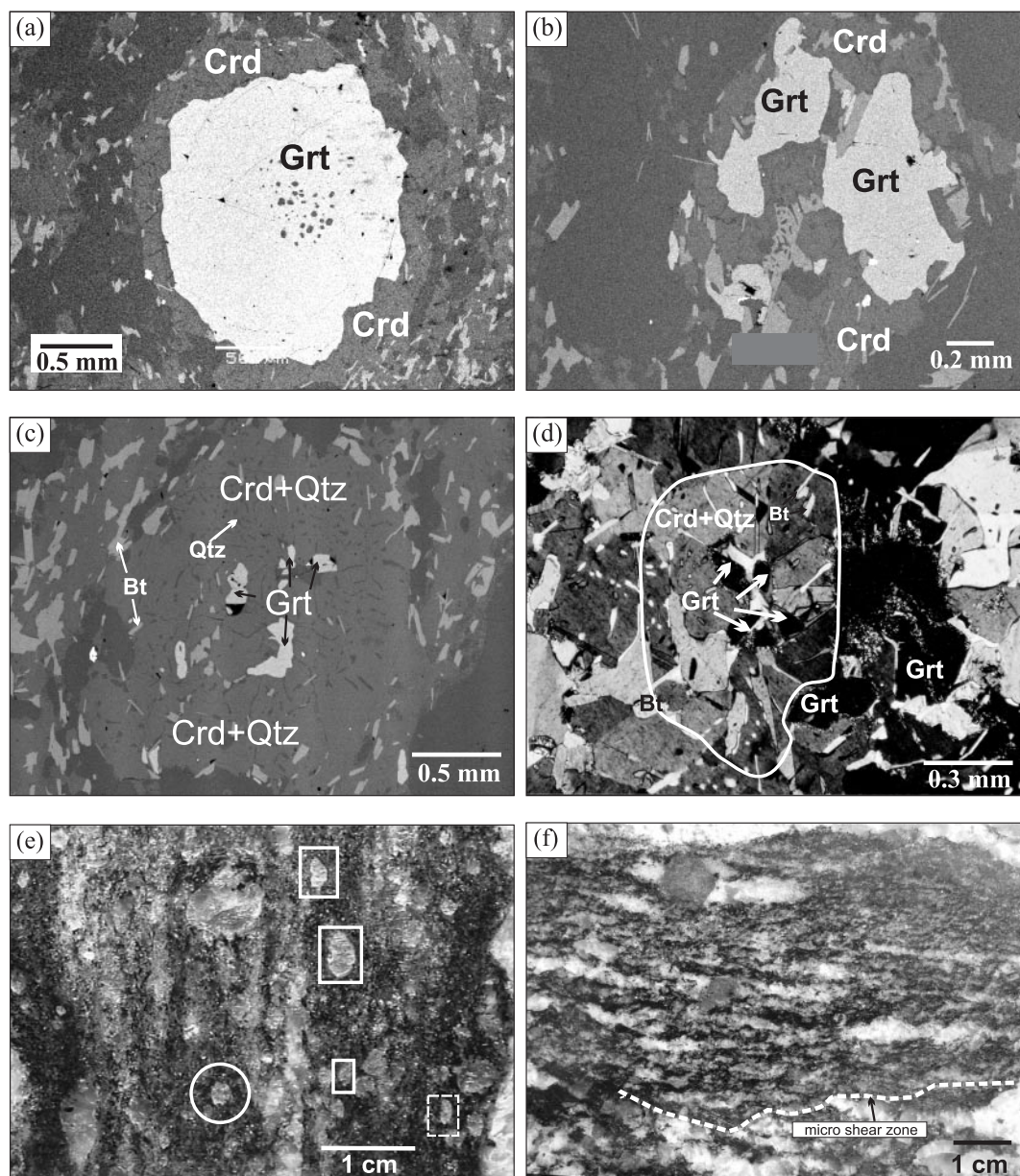


**Fig. 4.** (a–c) BSI of different stages of the replacement of garnet (+  $\text{Sil}_1$  + Qtz) by cordierite in sample T20. (d) Microphotograph (crossed polars) of the Crd + Qtz myrmekite-like symplectite reflects the same area as that of (c) in the thin section of sample T20. (e) and (f) are photographs of polished surfaces of samples T73 (e) and T20 (f) showing the  $D_2$  shear fabric enhanced by the presence of attenuated leucosomes (f) and trails of garnet (e). Garnets (in rectangles) are elongated (also Fig. 5) in the direction of the stretching mineral lineation. The circled area in (e) defines the position of (a). (f) also shows a Bt–Sil–Qtz micro shear zone that clearly follows the major foliation. (See text for details.)

or as euhedral porphyroblasts included in a fine-grained quartz–sillimanite–plagioclase schistose granoblastic matrix (Figs 3 and 4). Fresh cordierite forms porphyroblasts up to a few millimetres in size with well-developed twins. In other places cordierite mimics the morphology of the replaced garnet porphyroblasts (Fig. 4a). The cordierite porphyroblasts are commonly filled with sillimanite ( $\text{Sil}_1$ ) and/or quartz inclusions (Fig. 4d). Garnet forms both inclusion-free asymmetric grains elongated

along the  $S_3$  schistosity (Figs 3a and 5a–c) and atoll-shaped crystals (Fig. 3c). The formation of the asymmetric shape of garnet resulted from the replacement of elongated oval-shaped garnet porphyroblasts by cordierite from one side only, whereas the reaction-free side in contact with quartz and/or feldspar preserved the rounded primary shape. In sample T20 garnet is overgrown by well-developed cordierite–quartz symplectites (Fig. 4c and d). Backscattered images (BSI) in Fig. 4a–c

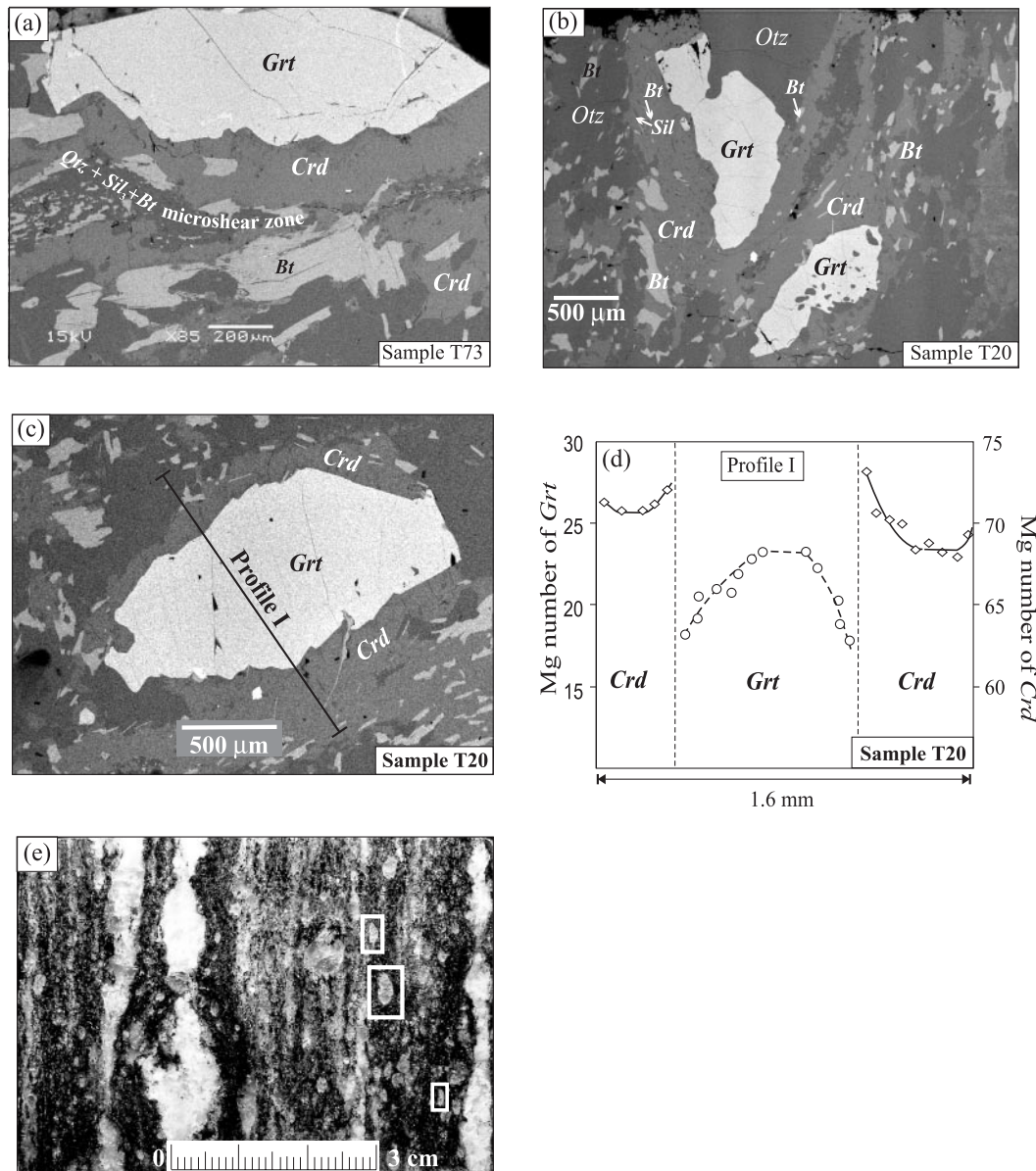
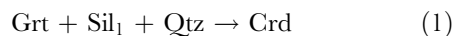


**Fig. 5.** Reaction textures of metapelites in T73 (a) and T20 (b, c) from the Baklykraal cross fold. (a) BSE of elongated garnet grain showing a 'hat' shape, which is the result of the different edges of the Grt being in contact with different minerals: the upper Grt edge is in contact with Qtz and reaction (1) is therefore absent, whereas the opposite side of the grain was presumably in contact with the matrix assemblage Bt + Sil + Qtz and was partially consumed by reaction (1) during the exhumation; it should be noted that the micro shear zone is oriented parallel to both the elongated Grt edge and the major foliation. (b) also demonstrates relict Grt whose elongated shape is caused by reaction (1). (d) Microprobe profile I reflecting the shift of exchange reaction (3) to the right side with falling temperature. (e) Photograph of the polished surface of sample T73 showing elongated shapes of garnet (rectangles) [compare with (a)].

demonstrate a systematic replacement of garnet by cordierite after the net-transfer divariant reaction



which is a typical characteristic of many metapelites from both the Central Zone and Southern Marginal Zone of the Limpopo Complex (e.g. Harris & Holland, 1984; Van Reenen *et al.*, 1990). In some thin sections

garnet porphyroblasts contain inclusions of quartz, plagioclase, and biotite. Micron-size inclusions of sillimanite are present in quartz porphyroblasts and millimetre-size sillimanite (Sil<sub>1</sub>) inclusions occur in both garnet and cordierite porphyroblasts. In sample T20 a few grains of Sil<sub>2</sub> occur in corona textures, whereas Sil<sub>3</sub> composes up to 90 modal % of the above-mentioned micro shear zones (e.g. Fig. 4f). Rare K-feldspar,

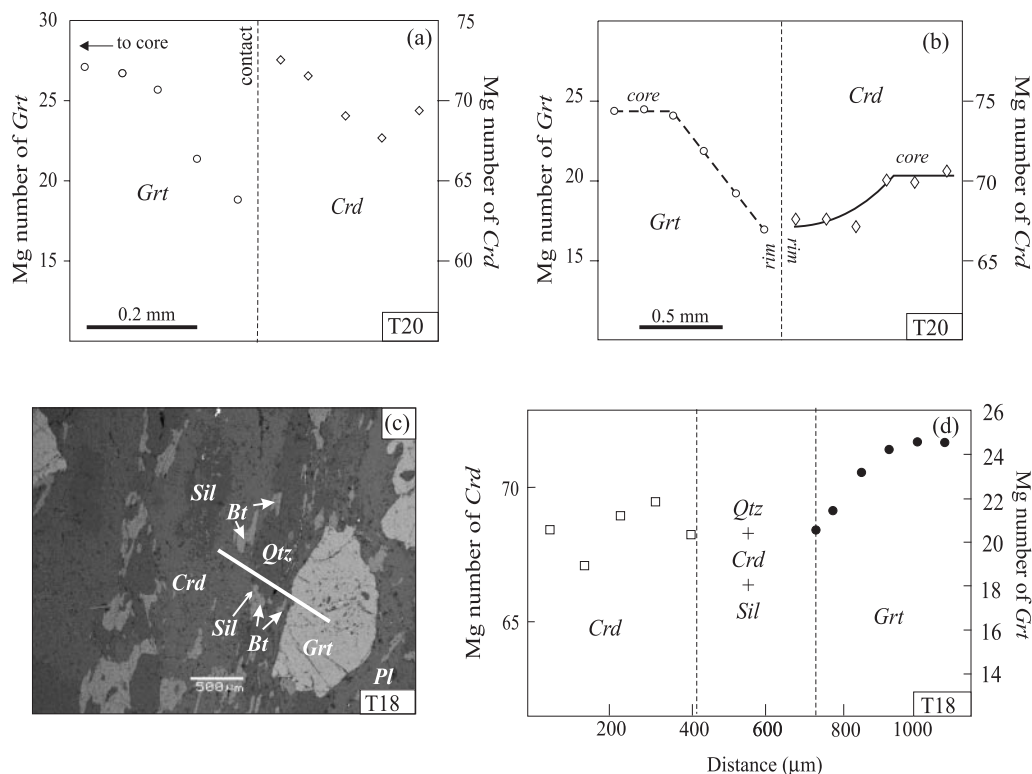
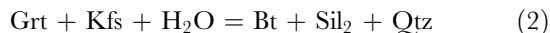


**Fig. 6.** Systematic zoning of garnet (a) in direct contact with cordierite, and (b) across a large cordierite porphyroblast that grew after garnet in samples T20 and T18. Microprobe profile (d) is across a 0.6 mm garnet grain separated from cordierite by the Qtz + Bt + Sil rim [see BSE in (c)]. In contrast to the profile in (a), which reflects the Fe–Mg exchange between Crd and Grt in their direct contact, profiles (b) and (d) illustrate a weak shift of reaction (1) to the right side with decreasing  $P$  and falling  $T$ , and, as a consequence, both garnet and cordierite become slightly Fe-rich.

Or<sub>94–100</sub> (Table 2), is present in all studied metapelites together with biotite, sillimanite (Sil<sub>2</sub>) and quartz. In a few cases we observed K-feldspar in paragenesis with garnet, but never with both cordierite and garnet, suggesting the displacement of the net-transfer reaction (1) and the reaction



to the right side. Biotite occurs in three generations: (1) as a matrix mineral or as separate elongated tabular grains coexisting with euhedral K-feldspar and quartz (sample T73); (2) in intergrowth with Sil<sub>2</sub> and Qtz (Fig. 3a–c); (3) in the fine-grained Bt + Qtz + Sil<sub>3</sub> assemblage of the micro shear zones (Figs 3a and 4f). In places the second generation of biotite separates cordierite from relic garnet (Fig. 3c), suggesting the replacement of primary Kfs as a result of its reaction with garnet in the presence of cordierite. Elongated quartz grains (5 mm long) are oriented parallel to the foliation and may also contain inclusions of sillimanite (Sil<sub>1</sub>) and saganitic rutile. A few late muscovite grains were observed within the newly formed Bt + Qtz + Sil<sub>2</sub> intergrowths in samples T73 and T18. The composition

of muscovite corresponds to its theoretical formula; no paragonite content was estimated.

In summary, the metapelites from the Baklykraal cross fold show the following three distinct features that developed during  $D_3/M_3$ : (1) systematic replacement of garnet, quartz and Sil<sub>1</sub> by cordierite after reaction (1); (2) the simultaneous development of the Bt + Qtz + Sil<sub>2</sub> assemblage instead of the Grt + Kfs paragenesis suggesting reaction (2), a typical retrograde hydration reaction; (3) the formation of the Bt + Qtz + Sil<sub>3</sub> assemblage that characterizes the micro shear zones, which probably relate to the latest stage of a single-stage retrograde metamorphism ( $M_3$ ).

### Reaction textures and mineral chemistry

From the previous section we can conclude that the relationship between minerals in metapelites from the Baklykraal cross fold is characterized by the widespread development of at least two major types of reaction textures: (1) replacement of garnet ( $\pm$  Sil<sub>1</sub> + Qtz) by cordierite (Figs 3–5); (2) replacement of the assemblage Grt + Kfs by the paragenesis Bt + Qtz + Sil<sub>2</sub> (Fig. 3). Both these ‘classical’ reaction textures reflect the retrograde stage of

Table 2: Standard thermodynamic data for some mineral reactions of the system  $FeO-MgO-SiO_2-Al_2O_3-K_2O-Na_2O-H_2O$  (Smit *et al.*, 2001)

No.	Reaction	$\Delta H^\circ$ (cal*)	$\Delta S^\circ$ (e.u)†	$\Delta V^\circ$ (cal/bar)
1	$\frac{1}{3}Prp + \frac{2}{3}Sil + \frac{5}{6}Qtz = \frac{1}{2}Crd_{Mg}$	51	4.620	0.63827
2	$Prp + San + H_2O = Phl + Sil + 2Qtz$	-23595	-31.214	0.547
3	$\frac{1}{3}Prp + \frac{1}{2}Crd_{Fe} = \frac{1}{3}Alm + \frac{1}{2}Crd_{Mg}$	-6134	-2.668	-0.03535
4	$\frac{1}{3}Prp + \frac{1}{3}Ann = \frac{1}{3}Alm + \frac{1}{3}Phl$	-7843	-5.699	0.025
5	$Ann + Crd_{Mg} = Crd_{Fe} + Phl$	-17461	-28.546	0.58235

\*1 cal = 4.1868 J.

†1 e.u. = cal bar/K.

metamorphism (e.g. Harley, 1989) and provide a key for estimating the  $P-T-a_{H_2O}^{fluid}$  conditions during exhumation of the granulite-facies rocks. In the Petrography section we showed that these shear zones also occur in other rock types of the Baklykraal cross fold. Similar micro shear zones also are characteristic of many granulite-facies terrains including the SMZ and the NMZ of the Limpopo Complex.

To calculate the thermodynamic parameters we used the method of systematic microprobe profiling of the minerals forming a reaction texture (e.g. Perchuk *et al.*, 2000). Minerals were analysed using a CAMECA electron microprobe at the Rand Afrikaans University (Johannesburg, South Africa) and a CAMECA SX50 at both the Ruhr University (Bochum, Germany) and the Department of Petrology at Moscow State University (Russia).

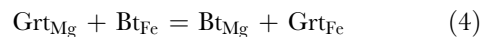
Selected microprobe analyses for representative profiles, the majority of which relate to the reaction textures, or to coexisting Fe-Mg minerals that are in contact with each other, are provided in Tables A1 and A2, which can be downloaded from the *Journal of Petrology* website at <http://www.oupjournals.org>. Figures 3, 5d and 6 demonstrate chemical profiles of contacting cordierites and garnets. In addition, for the purpose of thermobarometry we have analysed garnet and cordierite porphyroblasts from the sillimanite (Sil<sub>1</sub>) quartz matrix to avoid possible Fe-Mg diffusional exchange in the course of the net-transfer reaction (1).

Zoning profiles (Fig. 3) reflect the redistribution of Mg and Fe between cordierite and garnet according to the exchange reaction



which shifts to the right side with falling temperature (Perchuk, 1969, 1977). The shapes of the compositional profiles for garnet and cordierite in contact with each other reflect the crystallization of minerals in the four-phase field (Grt + Sil<sub>1</sub> + Qtz + Crd) during the progress

of reactions (1) and (3). For example, a large grain of garnet along profile IV (Fig. 3g) is isolated from cordierite by a narrow Qtz + Sil<sub>2</sub> ± Bt symplectitic zone (Fig. 3c), which results in a decrease of the Mg-numbers of garnet and cordierite towards their rims (Perchuk, 1969, 1977). This profile also may reflect a shift to the right of both the net-transfer reaction (2) and the associated (simultaneously operating) exchange reaction



during the retrograde stage of metamorphism. Therefore, we analysed the compositions of coexisting minerals in each sample chosen for thermobarometry. Reaction (2) is the divariant portion of the Opx-free Grt + Crd + Kfs + H<sub>2</sub>O = Bt + Sil<sub>2</sub> + Qtz univariant equilibrium of the KFMASH system. A systematic replacement of garnet by both cordierite and the Bt + Sil<sub>2</sub> + Qtz assemblage (e.g. Fig. 3c) suggests that K-feldspar has been largely consumed in the course of retrograde metamorphism.

The Mg-number of garnets from samples T73 (Table A1) and T20 (see Table 4) varies between 13 (rims) and 24 (cores), whereas in metapelite T18 marginal portions of Grt porphyroblasts have slightly higher  $N_{Mg}$  (~20) whereas the same  $N_{Mg}$  (24) is preserved in cores (see Table 4). The Ca content of garnet is low and decreases from core to rim. This is a common feature for retrograde granulites because of the breakdown of the grossularite component of garnet to produce anorthitic plagioclase, quartz and sillimanite (Newton & Haselton, 1981). In contrast, the low Mn content of garnet shows no systematic change from cores to rims of Grt porphyroblasts. Similar to garnet, cordierite in sample T18 shows a higher  $N_{Mg}$  (66–70, for rim to core, respectively) compared with samples T73 and T20 (61–66, for rim to core, respectively). Thus, the rims of the T18 cordierite have the same  $N_{Mg}$  as the cordierite cores in samples T73 and T20, a very unusual feature of metapelites sampled from

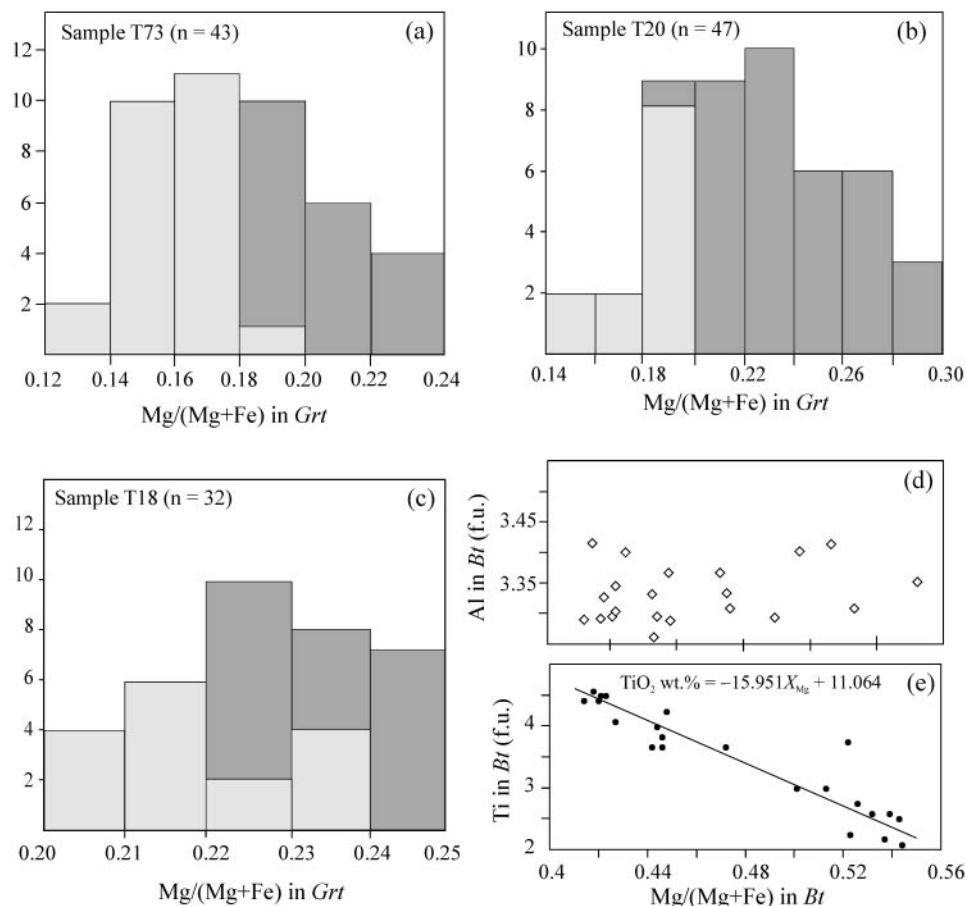


**Fig. 7.** Histograms showing some compositional characteristics of garnet (a–c) and biotite (d) from metapelites of the Baklykraal structure. Dark grey defines cores; light grey reflects distribution of  $X_{\text{Mg}}^{\text{Grt}}$  for rims. It should be noted that (1) all histograms show only one peak, and (2) there is no correlation between Al and  $X_{\text{Mg}}^{\text{Bt}}$  (d), and a strong negative correlation between  $\text{TiO}_2$  and  $X_{\text{Mg}}^{\text{Bt}}$  (e). The chemical data in this figure indicate that the formation and evolution of minerals may reflect a single metamorphic event.

the same geological structure. This compositional difference reflects a significant difference in temperature of the Grt–Crd equilibrium (Perchuk, 1977) because the  $N_{\text{Mg}}^{\text{Grt}}$  (24) in the cores of all samples reflects identical pressure conditions. The direct contacts of garnet with cordierite are characterized by a slight decrease of  $N_{\text{Mg}}^{\text{Grt}}$  (1–2), and an increase of  $N_{\text{Mg}}^{\text{Crd}}$  (62–66) (e.g. Fig. 3d–f, profiles I–III). A large, about 5 mm, atoll garnet was analysed from core to rim along Profile III in Fig. 3f.  $N_{\text{Mg}}^{\text{Grt}}$  varies from 24 (core) to 16 (rim), whereas  $N_{\text{Mg}}^{\text{Crd}}$  is fairly constant in the core (~62–63) and increases to the rim (up to 66) in contact with garnet. Several contacting grains of cordierite and garnet were analysed along profile IV (Fig. 3g). The major features of this profile are the following: (1) a decrease of  $N_{\text{Mg}}^{\text{Crd}}$  and  $N_{\text{Mg}}^{\text{Grt}}$  where the garnet and cordierite are separated by thin (50  $\mu\text{m}$ ) intergrowths of Qtz and Sil<sub>2</sub> (Fig. 3g), demonstrating a shift to the right of reaction (1); (2) absence of systematic chemical zoning in cordierite in contact with garnet (Fig. 3g).

The studied mineral assemblages and their chemical features are thus well suited to correctly decipher the  $P$ – $T$

history of the Baklykraal cross fold, if the potential pitfalls are taken into consideration. The samples represent both high- and low-strain coarse-grained rocks in which Grt and Crd grain sizes may exceed 1 mm, and contain reaction textures extensively developed after garnet (Figs 2 and 3). Histograms in Figure 7a–c show that in spite of the near-normal (Fig. 7a and b) or log-normal (Fig. 7c) distributions of  $N_{\text{Mg}}$ , the data demonstrate only one peak. This suggests that the garnet in the studied metapelites represents a single generation. In addition, zoning profiles of Grt and Crd have clear central plateaux with consistent compositions (Figs 4–6) that are considered to represent the highest  $P$ – $T$  conditions. Whereas both the garnet and K-feldspar are being consumed in reactions (1) and (2), some other minerals are present in the reaction textures in two continuous generations (e.g.  $\text{Bt}_1 \rightarrow \text{Bt}_2$ ,  $\text{Sil}_1 \rightarrow \text{Sil}_2$ ). This is clearly exemplified by Fig. 7d, where the  $\text{TiO}_2$  content of biotite decreases systematically with  $N_{\text{Mg}}^{\text{Bt}}$ , and, therefore, with fall in temperature (see Fig. 12c and d). This also follows from chemical zoning of biotites showing a decrease in  $\text{TiO}_2$  from the

core through the margin to the rim; for example, 4.5 → 3.6 → 3.0 wt % (see Table A2). Thus, the composition of biotite changes continuously from the peak Bt<sub>1</sub> to Bt<sub>2</sub> in the course of the progress of reaction (4).

In the Petrography section we mentioned that no reaction textures related to reaction (2) were observed because of almost total consumption of K-feldspar presented by Or<sub>100-95</sub> (Table A2). We measured several biotite–garnet pairs in contact with Qtz and Sil<sub>2</sub> that are associated with K-feldspar (Tables A1 and A2). Biotite has a relatively narrow range in composition and shows a strong negative Ti–Mg correlation (Fig. 7d): TiO<sub>2</sub> (wt %) = –15.951  $X_{Mg}$  + 11.064 (within the limits of data from Table A2), whereas the Al content shows no correlation with  $X_{Mg}^{Bt}$  (Fig. 7e) at an almost constant composition of K-feldspar (Table A2).

Profiles I–III (Fig. 3) reflect the progress of reaction (3), whereas profile IV demonstrates a very complex chemical zoning because the quartz–sillimanite intergrowth around cordierite may not be in direct contact with garnet, although some sillimanite (Sil<sub>1</sub>) and quartz occur as inclusions in garnet. The coexistence of minerals with both types of zoning profiles reflects the simultaneous operation of both reactions (1) and (3).

## THERMODYNAMICS OF METAMORPHISM

In this section we utilize the mineral chemistry from the studied rocks to understand the thermal and dynamic history of exhumation and emplacement of the Baklykraal cross fold. For this purpose we will use mineral relationships in the metapelites (Figs 3–6) and the observed changes in their compositions with pressure and temperature on the basis of the method described in detail by Perchuk *et al.* (2000, and references therein) and Smit *et al.* (2001).

### Mineral thermodynamics

We use an internally consistent dataset on mineral thermodynamics for the system FeO–MgO–SiO<sub>2</sub>–Al<sub>2</sub>O<sub>3</sub>–K<sub>2</sub>O–Na<sub>2</sub>O–H<sub>2</sub>O, which is derived from detailed experimental data aimed at the calibration of a set of geothermobarometers (Zyrianov *et al.*, 1978; Perchuk & Lavrent'eva, 1983; Aranovich & Podlesskii, 1989). Standard state data for the end-member reactions (1)–(4) are given in Table 2. Mixing properties of the mineral solid solutions of the reactions are taken from Gerya & Perchuk (1994).

#### Mg–Fe cordierite

It should be mentioned that reaction (1) noticeably depends on the water content of cordierite (Newton,

1972). To account for H<sub>2</sub>O and CO<sub>2</sub> solubility in cordierite Aranovich & Podlesskii (1989) suggested a garnet-like solid solution model:

$$(G_{Mg}^m)^{Crd} = 2RT \ln X_{Mg}^{Crd} + Q \quad (5)$$

$$(G_{Fe}^m)^{Crd} = 2RT \ln X_{Fe}^{Crd} + Q \quad (6)$$

where  $T$  is in Kelvin and  $Q$  is a correction parameter for thermal and baric solubility of H<sub>2</sub>O and CO<sub>2</sub> in cordierite:

$$Q = -1333 + 0.617T \text{ (K)} - 0.336P \text{ (kbar)} \\ + 1026(1 - X_{H_2O}^{fluid}) + 472(1 - X_{H_2O}^{fluid})^2 \quad (7)$$

where  $X_{H_2O}^{fluid} \approx a_{H_2O}^{fluid}$  because the concentration of water in Crd is unknown. Substituting the term  $Q$  in formulae (5) and (6) using equation (7) we obtain

$$G_{Mg-Crd}^m = RT \ln a_{Mg}^{Crd} = 2RT \ln X_{Mg}^{Crd} \\ - 1333 + 0.617T - 0.336P + 1026(1 - X_{H_2O}^{fluid}) \\ + 472(1 - X_{H_2O}^{fluid})^2 \quad (8)$$

$$G_{Fe-Crd}^m = RT \ln a_{Fe}^{Crd} \\ = 2RT \ln X_{Fe}^{Crd} - 1333 + 0.617T - 0.336P \\ + 1026(1 - X_{H_2O}^{fluid}) + 472(1 - X_{H_2O}^{fluid})^2. \quad (9)$$

#### Pyrope–almandine solid solution

$$G_{Prp}^m = RT \ln a_{Prp}^{Grt} = 3RT \ln X_{Mg}^{Grt} \quad (10)$$

$$G_{Alm}^m = RT \ln a_{Alm}^{Grt} = 3RT \ln X_{Fe}^{Grt}. \quad (11)$$

#### Biotite

Partial molar Gibbs mixing free energies of biotite solid solution

$$G_{Phl}^m = 3RT \ln X_{Phl}^{Bt} + (G_{Phl}^c)^{Bt} \quad (12)$$

$$G_{Ann}^m = 3RT \ln X_{Ann}^{Bt} + (G_{Ann}^c)^{Bt} \quad (13)$$

take into account both the Fe–Al and the Mg–Al interaction energies. Interaction parameters were calculated from the integral molar Gibbs excess free energy for the biotite solid solution using the following formula (Gerya & Perchuk, 1994):

$$G^c(\text{Bt}) = W_{MgAl}^G X_{Phl} X_{Eas} + W_{FeAl}^G X_{Ann} X_{Eas} \quad (14)$$

Table 3: P–T and compositional parameters of coexisting Bt, Grt and Kfs used for  $H_2O$  activity calculations in a fluid phase after reaction (3)

Bt	Grt	Kfs	$X_{Mg}^{Bt}$	$X_{Alm}^{Grt}$	$X_{Or}^{Fsp}$	$P$ (kbar)*	$T$ (°C)	$a_{H_2O}^{fluid}$
<i>Sample T73</i>								
95-1 c	95 c	95	0.446	0.174	1.0	4	660	0.371
95-2 c	95 c	95	0.446	0.174	1.0	4	659	0.332
95-2 c	95 r2	90	0.444	0.176	1.0	3	615	0.379
96-3	34	90	0.442	0.228	1.0	6	751	0.331
91	95 r1	90	0.501	0.148	1.0	3	573	0.363
<i>Sample T20</i>								
32 c	31 c	104	0.539	0.236	0.943	4	663	0.274
32 r	31 r (Qtz)	107	0.551	0.184	0.943	4	597	0.278
32 r	31 r (Bt)	107	0.551	0.183	0.943	3	580	0.274
43 c	42 c	107	0.551	0.272	0.943	5	697	0.252
43 c	42 2	104	0.551	0.267	0.943	5	690	0.253
43 c	42 3	107	0.551	0.257	0.943	5	677	0.248
43 c	42 r (Qtz)	107	0.551	0.210	0.943	4	619	0.276
46 c	45 c	107	0.542	0.217	0.943	4	636	0.281
48 c	48 c	104	0.532	0.214	0.943	4	640	0.276
108	110 c	107	0.522	0.270	0.943	5	724	0.263
108	109 r	107	0.522	0.231	0.943	4	673	0.283
105 c	106 r	107	0.504	0.192	0.943	4	635	0.306
46 c	42 r2	104	0.542	0.185	0.943	3	593	0.312
<i>Sample T18</i>								
1 c	4 c	2 c	0.526	0.225	0.962	4	659	0.294
1 r (Kfs)	4 r	2 r	0.523	0.219	0.972	4	654	0.294
6 c	7 c	5	0.539	0.225	0.962	4	659	0.274
6 r	7 r (Pl)	5	0.543	0.201	0.972	4	614	0.271
23 r	24 r	22	0.532	0.201	0.965	4	667	0.280
23 c	24 c	22	0.537	0.190	0.965	4	653	0.299
1 r (Qtz)	4 r	2 r	0.544	0.219	0.972	4	636	0.260

\*Conventional values that were calculated for reaction (1) involving dry cordierite because pressure effect is negligible on  $H_2O$  activity (see text for further explanation).  
c, core; r, rim.

where the Margules parameters are  $W_{MgAl}^G = -4405$  cal/mol and  $W_{FeAl}^G = -24577$  cal/mol, respectively. Molar fractions  $X_{Phl}$ ,  $X_{Ann}$  and  $X_{Eas}$  were calculated with the following formulae:

$$X_{Phl}^{Bt} = Mg/[Mg + Fe + 0.5(Al - 1)] \quad (15)$$

$$X_{Ann}^{Bt} = Fe/[Mg + Fe + 0.5(Al - 1)] \quad (16)$$

$$X_{Eas}^{Bt} = 0.5(Al - 1)/[Mg + Fe + 0.5(Al - 1)] \quad (17)$$

where  $X_{Phl}^{Bt} + X_{Ann}^{Bt} + X_{Eas}^{Bt} = 1$ .

### *K-feldspar*

A sub-regular model for the high albite–sanidine solid solution (Zyrianov *et al.*, 1978) can be used for calculations of  $a_{H_2O}^{fluid}$  via reaction (2) by the use of compositions of K-feldspar (Table 3) in direct contact with the Bt + Sil<sub>2</sub> + Qtz assemblage developed around garnet (e.g. Fig. 3g).

Using these mixing properties and standard state thermodynamic data from Table 2 we have calculated the  $T$ – $P$ – $\mathcal{N}_{Mg}$  phase diagram for divariant equilibrium (1). Figure 8 demonstrates an isothermal (700°C)  $P$ – $\mathcal{N}_{Mg}$  diagram. All the discussed properties and data of Table 2 allow calculation of the  $T$ – $P$ – $a_{H_2O}^{fluid}$  parameters for local

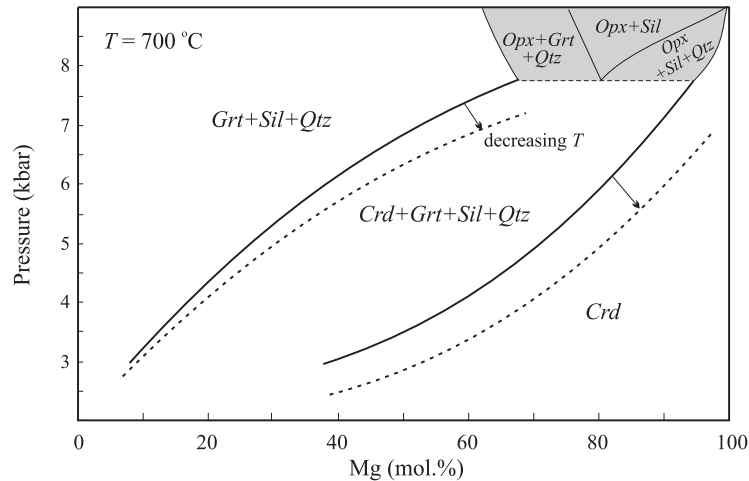


**Fig. 8.** Isothermal section of the  $T$ - $P$ - $N_{\text{Mg}}$  diagram for the divariant equilibrium (1) calculated at  $a_{\text{Crd}} = 1.0$  (Aranovich & Podlesskii, 1989) using standard thermodynamic data from Table 2 and mixing properties of Crd and Grt from equations (7)–(13). The shaded area indicates phase relationships in the Crd-free field calculated using data on Opx thermodynamics from the paper by Smit *et al.* (2001). It should be noted that both the Crd and coexisting Grt become more Mg-rich with falling temperature (dashed lines).

mineral equilibria in metapelites of the Baklykraal cross fold.

### $P$ - $T$ paths

Because  $P$ - $T$  paths are the basis for geodynamic speculations, the method of their derivation will always be important. For the past two decades, workers have used different approaches for constructing  $P$ - $T$  paths with the result that published  $P$ - $T$  trajectories for the same geological unit may have different shapes. Also,  $P$ - $T$  paths from complexly deformed high-grade terrains cannot be accurately derived without integrating petrological and structural data. The CZ of the Limpopo Complex is one of the best examples of controversies concerning both the shapes of published  $P$ - $T$  paths and their geodynamic interpretation.

Detailed paragenetic analysis of widely developed retrograde Crd-bearing mineral assemblages in aluminous rocks from different parts of the CZ in South Africa and Botswana led to the conclusion that isothermal-decompression (ITD) (Horrocks, 1983; Harris & Holland, 1984; Windley *et al.*, 1984; Droop, 1989; Van Reenen *et al.*, 1990), isobaric cooling (IBC) combined with ITD (Tsunogai *et al.*, 1992; Hisada & Miyano, 1996), or decompressional-cooling (DC) (Perchuk *et al.*, 1996, 2000)  $P$ - $T$  paths reflect a single exhumation event. Holzer *et al.* (1998), on the other hand, proposed two contrasting  $P$ - $T$  paths for the evolution of the Central Zone: an anticlockwise  $P$ - $T$  path reflecting a Late Archaean ( $\sim 2.6$ – $2.55$  Ga) low-pressure granulite-facies metamorphism associated with voluminous granitic and charnockitic plutonism, and a Proterozoic ( $\sim 2.0$  Ga) high-pressure ITD path. Evidence for the anticlockwise

$P$ - $T$  path is based mainly on the results of unpublished data (Holzer, 1995) from metapelitic gneisses from the ‘Three Sisters’ area on the farm Boston, about 20 km WNW of Messina, in which rectangular sillimanite was interpreted to reflect pseudomorphs after andalusite.

In the following section we will derive a  $P$ - $T$  path for metapelites from the Baklykraal cross fold based on reaction textures and mineral chemistry (Tables 2 and A2), and on the  $P$ - $T$ - $a_{\text{H}_2\text{O}}^{\text{fluid}}$  dataset (Tables 3 and 4) to demonstrate the coherence of the thermodynamic results with the discussed structural evolution of this cross fold.

### Thermobarometric studies and $\text{H}_2\text{O}$ activity calculations

Thermobarometry of granulites is recognized as a complex problem because of the high-temperature conditions and strong recrystallization of rocks at peak metamorphic conditions that obliterate most compositional and textural evidence for the pre-peak history. Therefore, in most cases only retrograde  $P$ - $T$  paths are documented for granulites based on reaction textures and chemical zoning of coexisting minerals (e.g. Perchuk, 1985, 1989; Harley, 1989). In addition, many ion-exchange geothermometers have apparent closure temperatures below those of granulite-facies conditions, causing difficulties in obtaining  $P$ - $T$  parameters of peak metamorphic conditions for granulite-facies terrains. Several workers (e.g. Frost & Chacko, 1989; Harley, 1989; Spear & Florence, 1992; Spear, 1993) have also noted that geothermometers based on Fe–Mg exchange reactions are not likely to quench at the same  $P$ - $T$  conditions as geobarometers that are based on net-transfer reactions. Therefore, in several cases, retrograde  $P$ - $T$  paths of

Table 4: Compositional and thermodynamic parameters used for deriving the  $P$ - $T$  paths

Figure no.	$N_{Mg}^{Crd}$	$N_{Mg}^{Grt}$	$T$ ( $^{\circ}C$ )	$a_{H_2O}^{fluid}$	$P$ (kbar)
<i>Sample T73</i>					
3f	0.614	0.231	786	0.325	5.68
3f	0.625	0.237	781	0.326	5.69
3f	0.614	0.228	779	0.327	5.59
3f	0.640	0.228	740	0.335	5.22
3f	0.623	0.214	736	0.336	5.05
3f	0.611	0.208	727	0.338	4.90
3f	0.632	0.208	712	0.342	4.76
3f	0.629	0.205	710	0.342	4.72
3f	0.626	0.202	708	0.343	4.68
3f	0.623	0.200	708	0.343	4.66
3g	0.627	0.203	708	0.343	4.69
3g	0.612	0.189	700	0.344	4.48
3g	0.629	0.196	692	0.346	4.46
3g	0.620	0.188	688	0.347	4.33
3g	0.627	0.191	685	0.348	4.34
3g	0.610	0.178	679	0.349	4.14
3g	0.620	0.184	679	0.349	4.21
3g	0.637	0.194	678	0.349	4.30
3g	0.620	0.179	669	0.351	4.06
3g	0.620	0.177	665	0.352	3.99
3e	0.632	0.181	658	0.354	3.98
3e	0.614	0.168	653	0.355	3.78
3e	0.620	0.168	646	0.357	3.72
3d	0.645	0.180	640	0.358	3.81
3d	0.659	0.180	623	0.362	3.66
3d	0.621	0.156	620	0.362	3.33
3d	0.621	0.146	599	0.367	3.02
3d	0.629	0.146	591	0.369	2.95
<i>Sample T20</i>					
6b	0.628	0.248	788	0.284	5.84
6b	0.630	0.218	729	0.308	5.01
6b	0.628	0.218	732	0.307	5.03
6b	0.632	0.211	713	0.314	4.80
6b	0.631	0.188	673	0.330	4.19
6b	0.630	0.185	668	0.333	4.11
6b	0.631	0.175	649	0.340	3.83
6b	0.628	0.160	623	0.350	3.43
6b	0.630	0.150	602	0.359	3.12
<i>Sample T18</i>					
6d	0.661	0.243	737	0.336	5.35
6d	0.681	0.230	685	0.348	4.77
6d	0.670	0.245	728	0.338	5.28
6d	0.681	0.205	641	0.358	4.15
6d	0.688	0.234	683	0.348	4.79

granulites deduced from thermobarometry using mineral compositions affected by late Fe–Mg exchange may give misleading results, representing apparent  $P$ - $T$  trajectories (e.g. Frost & Chacko, 1989; Spear & Florence, 1992; Spear, 1993). Frost & Chacko (1989) suggested several procedures to maximize the correct retrieval of peak metamorphic conditions and retrograde  $P$ - $T$  paths for granulites. The approach used by our group (Perchuk *et al.*, 1985, 1996, 2000; Smit *et al.*, 2001) for derivation of a  $P$ - $T$  path not only involves the majority of the above-mentioned procedures but also accounts for other methods such as numerical modelling of  $P$ - $T$  paths for rocks of high-grade terrains (e.g. Gerya *et al.*, 2000, 2002). Taking into account that different  $dT/dP$  slopes of  $P$ - $T$  paths are commonly associated with specific mineral reactions observed in granulites (e.g. Harley, 1989), a crucial step is the use of reaction textures to test  $P$ - $T$  trajectories of granulites (Perchuk *et al.*, 1989, 1996, 2000; Smit *et al.*, 2001).

For thermobarometric calculations we used an internally consistent thermodynamic dataset of Perchuk *et al.* (1985; see also Perchuk, 1990), calibrated on the basis of original experimental data on the mineral equilibria involving solid solutions of garnet, cordierite and biotite (Perchuk & Lavrent'eva, 1983; Aranovich & Podlesskii, 1989). The cordierite–garnet [reaction (3)] and the biotite–garnet [reaction (4)] exchange equilibria were used for the estimation of temperatures parameters, whereas reactions (1) and (3) were utilized for calculating the pressure and  $a_{H_2O}^{fluid}$ , respectively, for local mineral equilibria. At equilibrium conditions the Gibbs free energy is the following:

$$\Delta G_{(1)} = \Delta H_{(1)}^o - T\Delta S_{(1)}^o + P\Delta V_{(1)}^o + (G_{Mg}^m)^{Crd} + G_{Prp}^m = 0. \quad (18)$$

The  $X_{H_2O}^{fluid}$  can be calculated from the  $H_2O$  activity in a fluid. Because all studied metapelites of the Baklykraal area contain the Bt + Sil + Qtz + Kfs + Grt reaction texture, indicating reaction (2), we can apply the equation

$$a_{H_2O}^{fluid} = \exp[\Delta G_{(2)}/RT]$$

where

$$\Delta G_{(2)} = \Delta H_{(2)}^o - T\Delta S_{(2)}^o + P\Delta V_{(2)}^o + RT \ln f_{H_2O} - G_{Phl}^m + G_{Prp}^m + G_{San}^m. \quad (19)$$

The  $H_2O$  activity is a very sensitive parameter that ‘monitors’ the presence in rocks of mineral equilibria involving  $H_2O$ . If the compositional parameters at a given  $T$  and  $P$  are not correct, the calculated  $H_2O$  activity may change dramatically, e.g. from negative values to  $a_{H_2O}^{fluid} \gg 1$ . Therefore to calculate external

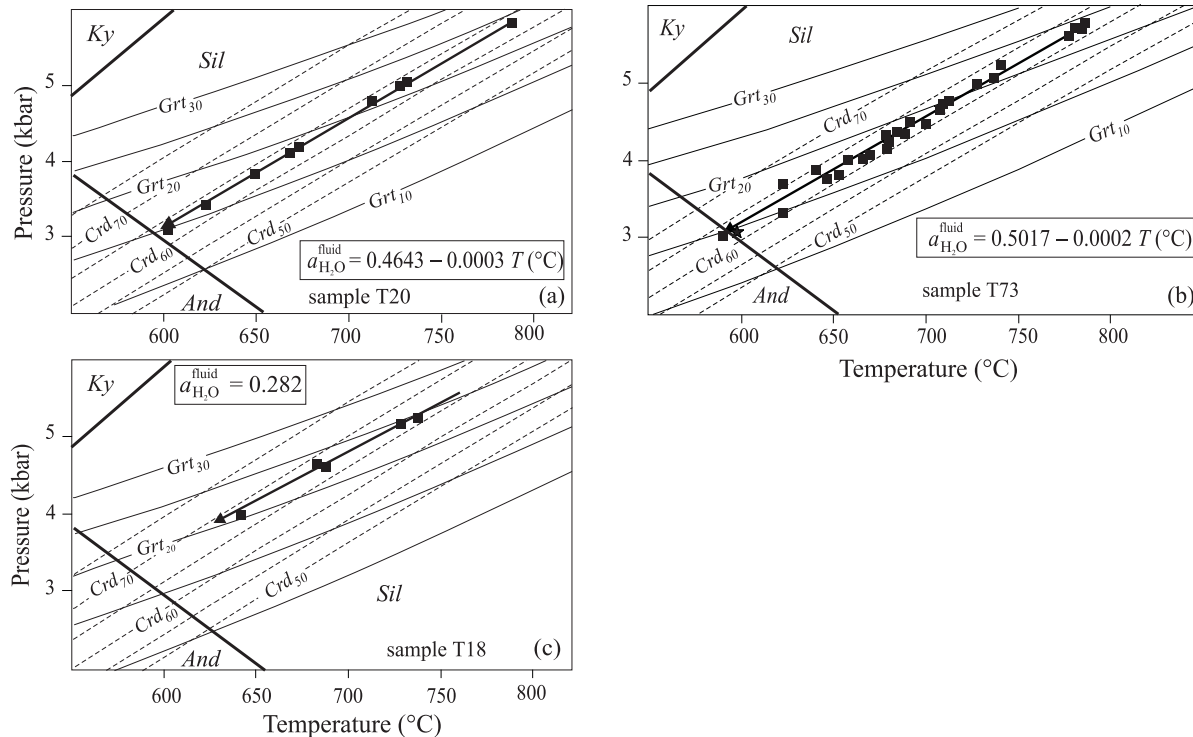


**Fig. 9.**  $P$ - $T$  paths (arrows) derived from compositions of coexisting garnet and cordierite associated with sillimanite and quartz in samples T20 (a), T73 (b), and T18 (c) (■). The Grt (continuous lines) and Crd (dashed lines) isopleths show the corresponding Mg-numbers. Both the isopleths and data points for each sample in (a)–(c) are calculated on the basis of thermodynamic data from Table 2 and mixing properties of Fe–Mg minerals (see text for further explanation). All data are taken from Table 4.

thermodynamic parameters ( $T$ ,  $P$  and  $a_{\text{H}_2\text{O}}^{\text{fluid}}$ ) of local equilibria for the derivation of the  $P$ - $T$  path, we have to use (1) an internally consistent thermodynamic database, and (2) the correct method of investigating the equilibrium compositions of coexisting minerals in metapelites from the Baklykraal cross fold.

The standard state thermodynamic data from Table 2, mixing properties from formulae (10)–(14) and the Ab–San solid solution model allow calculation of  $a_{\text{H}_2\text{O}}^{\text{fluid}}$  with equation (19) at a given  $T$  and  $P$ . There are two ways to do this. The first one is the joint solution of equations (18) and (19) at the temperature calculated with the Bt–Grt thermometer. The second way is based on the negligible contribution of the  $PAV^\circ$  term in  $\Delta G_{(3)}$ : the variation of  $P$  within 5 kbar results in a change of  $a_{\text{H}_2\text{O}}^{\text{fluid}}$  of not more than 0.005. Both methods show similar, or even identical results. Table 3 demonstrates the results for 29 Bt + Sil + Qtz + Kfs + Grt assemblages, which were described in the previous section (see Table A2).

However, because the  $\text{H}_2\text{O}$  activity depends on temperature, it is more practical to find analytical correlations between  $T$  and  $a_{\text{H}_2\text{O}}^{\text{fluid}}$  using data from Table 3.

Muscovite is a critical mineral in the studied metapelites in terms of the lowest temperature limits of the retrograde stage of metamorphism: it occurs very rarely

as a secondary phase after Fsp and Sil<sub>2</sub>. The upper temperature limit cannot be higher than 800°C (Spear *et al.*, 1999) because partial melting is not characteristic of the metapelites studied, and orthopyroxene is absent. Therefore reaction (2) proceeds within a relatively narrow  $P$ - $T$ - $a_{\text{H}_2\text{O}}^{\text{fluid}}$  range. We used this temperature range to make corrections for calculations of both cordierite and garnet isopleths and the determination of  $a_{\text{H}_2\text{O}}^{\text{fluid}}$  for each particular local equilibrium at temperatures estimated by the Bt–Grt thermometer. Using the data from Table 3 (some selected analyses are given in Tables A1 and A2) and taking into account that pressure has a negligible effect on the biotite–garnet thermometer, and in particular on the  $\text{H}_2\text{O}$  activity, we have approximated  $a_{\text{H}_2\text{O}}^{\text{fluid}}$  for sample T73 as a linear function of temperature (Fig. 9) within the interval 550–750°C:

$$a_{\text{H}_2\text{O}}^{\text{fluid}} = 0.5017 - 0.000224T \text{ (}^\circ\text{C)}. \quad (20)$$

Thus, equation (20) can be used for calculating both the  $P$ - $T$  path for T73 on the basis of mineral zoning (Table A1) preserved in the reaction textures (Figs 3 and 4), and isopleths ( $N_{\text{Mg}}^{\text{Grt}}$  and  $N_{\text{Mg}}^{\text{Crd}}$ ) on the  $P$ - $T$  plane of the system. A similar procedure was used for calculating  $a_{\text{H}_2\text{O}}^{\text{fluid}}$  for sample T20: it is approximated

by the following equation (see also Fig. 9):

$$a_{\text{H}_2\text{O}}^{\text{fluid}} = 0.4643 - 0.0002966T \text{ (}^\circ\text{C)}. \quad (21)$$

The free term of equation (21) differs slightly from that of equation (20), and the terms at  $T$  are very close. In contrast to samples T73 and T20, data for sample T18 (Table 3) show no systematic change of  $\text{H}_2\text{O}$  activity with temperature:  $a_{\text{H}_2\text{O}}^{\text{fluid}}$  varies within the limits 0.294–0.260, being very close to the  $a_{\text{H}_2\text{O}}^{\text{fluid}}$  calculated for sample T20. This very small change allows (1) assigning an average  $a_{\text{H}_2\text{O}}^{\text{fluid}}$  value, i.e. 0.282, or (2) integrating all values for sample T18 from Table 3 with the  $T$ – $a_{\text{H}_2\text{O}}^{\text{fluid}}$  data for sample T20. This integration gives a result that is almost identical to approximation (21):

$$a_{\text{H}_2\text{O}}^{\text{fluid}} = 0.4305 - 0.0002T \text{ (}^\circ\text{C)}. \quad (22)$$

Variations of  $\text{H}_2\text{O}$  activity also affect reaction (1), and this should be taken into account for calculations of both the  $\mathcal{N}_{\text{Mg}}^{\text{Grt}}$  and  $\mathcal{N}_{\text{Mg}}^{\text{Crd}}$  isopleths and the  $P$ – $T$  path derived from chemical zoning of coexisting minerals in the studied metapelites. Such a simple approach allows the calculation of Crd and Grt isopleths in the  $P$ – $T$  field for reaction (1) at a given  $a_{\text{H}_2\text{O}}^{\text{fluid}}$ , as well as  $P$ – $T$  parameters for the cordierite–garnet assemblages from local equilibria in the reaction textures (see Fig. 4). We also used the temperature interval of the evolution of the biotite–garnet equilibrium (see Table 3). Selected  $P$ – $T$  parameters for some local mineral equilibria are given in Tables 3 and 4.

### The method

For the accurate derivation of a  $P$ – $T$  path for the studied metapelites from the Baklykraal cross fold we used the procedure described in several papers (Perchuk *et al.*, 1985, 1989, 1996, 2000; Perchuk, 1987, 1989; Gerya & Perchuk, 1997; Gerya, 1999; Smit *et al.*, 2001) that involves the following major steps.

(1) *Microstructure studies.* The sequence of events related to the simultaneous growth of minerals in the reaction textures [e.g. reactions (1) and (2)] should be established.

(2) *Microprobe studies.* The chemical evolution of rock-forming minerals, involved in different types of reactions (e.g. net-transfer and exchange reactions), must be based on detailed microprobe profiling. This, however, should only be done after a preliminary microprobe study of relatively large porphyroblasts of garnet and other coexisting minerals involved in the reaction textures. A flat profile through the central portions of such porphyroblasts may indicate a peak of metamorphic conditions (e.g. Spear & Florence, 1992). This allows an understanding of the contribution of exchange [e.g. reactions (3) and (4)] and net-transfer reactions [e.g. reactions (1) and (2)] during the coherent change of mineral compositions in the course of exhumation.

(3) *Geothermobarometric calculations.*  $P$ – $T$  parameters for local equilibria should be calculated for the different stages of the formation of mineral assemblages using the ‘core–core rim–rim’ method. Mineral compositions of cores and rims can be selected using the results of the microprobe profiling, to avoid the influence of the latest exchange diffusion on barometry (e.g. Frost & Chacko, 1989; Spear & Florence, 1992). In the case of a cordierite-bearing equilibrium  $a_{\text{H}_2\text{O}}^{\text{fluid}} = f(T)$  must be calculated via a simultaneously operating reaction.

(4) *Derivation of a  $P$ – $T$  path.* A  $P$ – $T$  trajectory should be derived on the basis of individually calculated  $P$ – $T$  data for local mineral equilibria. The consistency of the  $P$ – $T$  trajectory must be tested with both mineral zoning (i.e. the relationship of the  $P$ – $T$  path with calculated compositional isopleths in observed divariant assemblages) and reaction textures.

(5) *Fluid inclusions test.* If fluid inclusion data for the studied samples are available, the combination of densities of the inclusions with mineral thermometry data can be used for the independent derivation of a  $P$ – $T$  path. Its comparison with the  $P$ – $T$  trajectory, derived from mineral thermobarometry only, may help to demonstrate the accuracy of the derivation (e.g. Perchuk *et al.*, 1985, 1989; Perchuk, 1987, 1989).

(6) *Mineral mode test.* It is recommended that the derived  $P$ – $T$  path be tested by calculating the Grt mode isopleths on the basis of bulk-rock compositions (e.g. Gerya, 1991, 1999; Perchuk *et al.*, 1996, 2000; Smit *et al.*, 2001), or using the polymineral modes (e.g. Carson *et al.*, 1999; Wei *et al.*, 2003).

(7) *Numerical test.* An additional test is that the derived  $P$ – $T$  path should conform to the results of numerical modelling (e.g. Gerya *et al.*, 2000, 2002).

(8) *Application.* The correct geological and geodynamic interpretation of the derived  $P$ – $T$  path.

Step (5) is useful, if well-developed reaction textures are absent from the particular metamorphic rock. Steps (7) and (8) can be extremely useful, if detailed structural and petrological data from major geological structures are integrated, such as is the case with the Baklykraal cross fold in the CZ of the Limpopo Complex.

### Derivation of a $P$ – $T$ path for the Baklykraal metapelites

Detailed microstructural studies are used to define the most appropriate reaction textures (see Figs 3–6) reflecting changing thermodynamic parameters. The systematic profiling of garnet porphyroblasts has been done for each studied sample with the aim of defining a maximal  $\mathcal{N}_{\text{Mg}}$  along a flat plateau [see step (2) in the previous subsection]. Histograms (a)–(c) in Fig. 7 demonstrate the distribution of  $\mathcal{N}_{\text{Mg}}$  for the central portions of relatively large (>0.5–1 mm) garnet porphyroblasts (e.g. Spear & Florence, 1992), and profiles in Figs 3, 5 and 7 show the  $\mathcal{N}_{\text{Mg}}$  plateaux for both Grt and Crd. Thus, we are

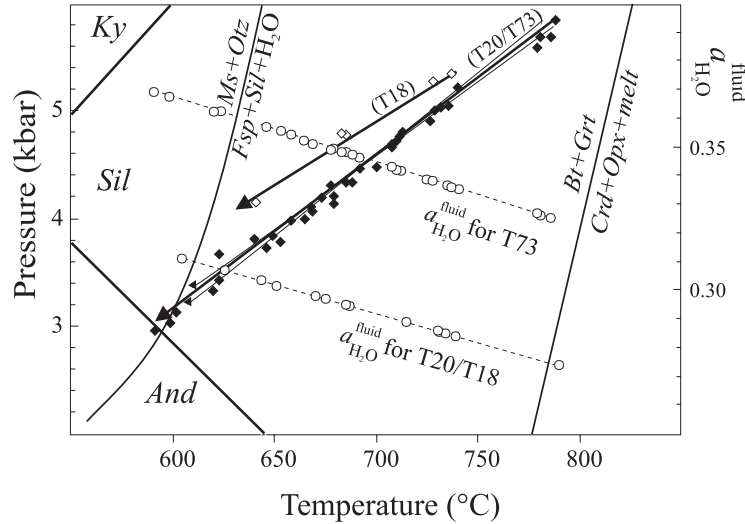


**Fig. 10.** Integrated  $P$ - $T$  path (bold arrows) reflecting the exhumation of granulites from the Baklykraal cross fold in the Central Zone of the Limpopo Complex. The fluid-absent melting reaction  $Bt + Qtz = Crd + Opx + melt$  is taken from Spear *et al.* (1999). The reaction  $Ms + Qtz = Fsp + Al_2SiO_5 + H_2O$  is calculated for  $a_{H_2O}^{fluid} = 0.3$ . Data points ( $\blacklozenge$ , samples T20 and T73;  $\diamond$ , sample T18) and corresponding  $P$ - $T$  trajectories (fine arrowed lines) are taken from Fig. 9a-c for comparison. The  $H_2O$  activity varies along the  $P$ - $T$  paths as a function of temperature only. Thin dashed lines and corresponding data points ( $\circ$ ), calculated after equations (20) and (22), are taken from Table 3. (For further explanation see the text.)

confident that the mineral compositions, equilibrated at near-peak metamorphic conditions, are correctly determined. Equilibrium compositions of rims were assumed for grains that are unaffected by very late exchange diffusion (Lasaga, 1983). Such rims are either isolated by the inert products of mineral reactions (e.g. Fig. 3g), or include rims that do not show typical diffusion profiles (Figs 3d-f, 6a, b and d).

A  $P$ - $T$  trajectory can be derived on the basis of  $P$ - $T$ - $a_{H_2O}^{fluid}$  data calculated individually for a particular local equilibrium. Therefore, the consistency of a  $P$ - $T$  path is controlled both by the mineral zoning (i.e. the relationship of the  $P$ - $T$  path with calculated isopleths for Grt, Crd, and Bt in the observed divariant assemblages), and by the reaction textures. However, in the cases of reactions (1) and (2) the isopleths on the  $P$ - $T$  plane should be projected from  $a_{H_2O}^{fluid}$ , i.e. the  $H_2O$  activity must vary along each particular isopleth in accordance with equations (20)–(22).

Thus, using individual  $P$ - $T$  estimates we deduced  $P$ - $T$  paths for three samples, T18, T73, and T20. Figure 9 demonstrates the results. All data points in the diagrams represent individual measurements of  $P$ - $T$  parameters and  $a_{H_2O}^{fluid}$  for the assemblage  $Crd + Grt + Sil + Qtz + Bt + Kfs$ , as given in Table 4. These  $P$ - $T$  paths are compared with  $N_{Mg}^{Crd}$  and  $N_{Mg}^{Grt}$  isopleths (Fig. 9) calculated using thermodynamic data for reactions (1) and (3) (Table 2) and our calibrations of  $a_{H_2O}^{fluid}$  as a function of temperature (corresponding equations are shown in Fig. 9a-c).

The  $P$ - $T$  path for sample T18 (Fig. 9a) slightly intersects both the garnet and the cordierite isopleths. The

$P$ - $T$ - $a_{H_2O}^{fluid}$  path for sample T73 (Fig. 9b) was derived on the basis of the  $P$ - $T$  data from Table 4. It follows the cordierite isopleth and cross-cuts the garnet isopleth, reflecting changes in  $N_{Mg}^{Grt}$  along a profile from the core to the rim (e.g. Fig. 3e and f). The T73  $P$ - $T$  path is very similar to that of sample T18. As mentioned above, all three diagrams are a complex projection of the  $Crd$ - $Grt$ - $Sil$ - $Qtz$  system onto the  $P$ - $T$  plane from  $a_{H_2O}^{fluid}$  and  $N_{Mg}$  of the Fe-Mg minerals. The cordierite in sample T20 demonstrates two types of chemical zoning (Figs 5 and 6): (1) an increase of  $N_{Mg}^{Crd}$  in direct contact with garnet in a reaction texture (Figs 5d and 6a); (2) a decrease of  $N_{Mg}^{Crd}$  in porphyroblasts included in the quartz-sillimanite ( $Sil_1$ ) matrix (Fig. 6b). Thus, we have the opportunity to check our statement on the simultaneous operation of reactions (1) and (3) in the studied samples by the derivation of  $P$ - $T$  paths on the basis of analytical data on: (1) profiling of the reaction texture (Fig. 4, contacting Grt and Crd with diffusion-like zoning); (2) non-contacting cordierite and garnet porphyroblasts (Fig. 6, with opposite  $N_{Mg}$  zoning) from sample T20. Both  $P$ - $T$  paths for this sample were derived at an identical  $a_{H_2O}^{fluid}$  and overlap each other completely, resulting in a single  $P$ - $T$  path (Fig. 9c). The  $P$ - $T$  paths also cross-cut three garnet isopleths reflecting changes in  $N_{Mg}^{Grt}$  along the profile from the core to rim of garnet (e.g. Figs 5d and 6a), whereas a decrease in the  $N_{Mg}^{Crd}$  is negligible (Fig. 9c, Table 4). The  $P$ - $T$  path is similar to that of samples T18 and T73 (Fig. 9a and b).

The  $P$ - $T$  diagram of Fig. 10 integrates all three trajectories into a single  $P$ - $T$  path for the metapelites from the

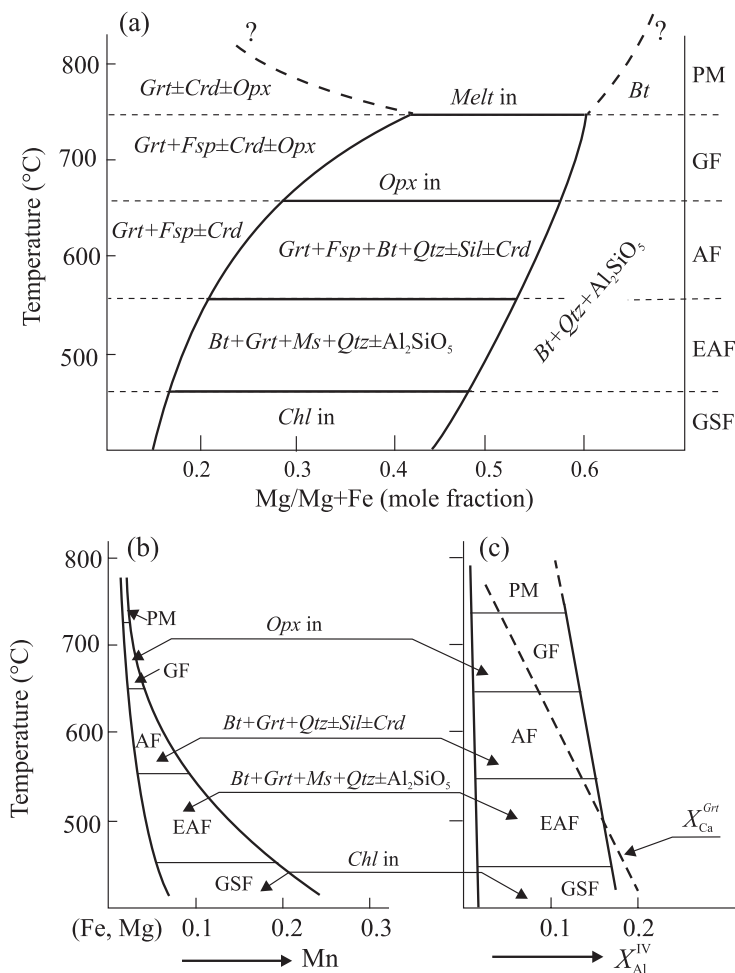


**Fig. 11.** Temperature–composition diagrams for the Bt–Grt assemblages collected from different metamorphic complexes [upgraded statistical data from Perchuk & Lavrent'eva (1983)]. Metapelites with the assemblage Bt + Sil + Qtz + Grt + Fsp + Crd dominate. The temperature is calculated from the Bt–Grt thermometer for average compositions of biotite and garnet at the boundaries dividing the facies. (a) shows the effect of falling temperature on an increase of both the partition coefficient ( $X_{Mg}^{Bt}/X_{Mg}^{Grt}$ ) for reaction (1) and the distribution coefficient for reaction (3). (b) and (c) demonstrate the significant changes of other compositional parameters of garnet (Mn, Ca,  $Al^{IV}$ ) in contrast to those of biotite. GSF, greenschist facies; EAF, epidote–amphibolite facies; AF, amphibolite facies; GF, granulite facies; PM, partial melting.

Baklykraal cross fold. The diagram also locates the  $P$ – $T$  path between major reactions that limit the field of stability at relatively low temperature by the Fsp + Sil paragenesis, and at relatively high temperatures by partial melting of the rocks. In the Petrography section we mentioned the presence of rare muscovite and the absence of partial melting reactions in the metapelites, thus supporting the correct position of the  $P$ – $T$  path in the diagram (Fig. 10).

#### Discussion of the derived $P$ – $T$ path

In this section we discuss two of the most important problems related to the calculated  $P$ – $T$  paths: (1) the reason for the linearity of the  $P$ – $T$  trajectory in Fig. 10; (2) the shape and direction of the  $P$ – $T$  path, i.e. the

question as to whether the trajectory resulted from DC or IBD.

(1) *The shape of the  $P$ – $T$  path derived in Fig. 10.* As mentioned before, near-linear  $P$ – $T$  trajectories have been the subject of much discussion over the last 15 years (e.g. Frost & Chacko, 1989; Harley, 1989; Spear & Florence, 1992; Spear, 1993; Smit *et al.*, 2001). Frost & Chacko (1989) attempted to prove that the linearity of a  $P$ – $T$  trajectory is an artefact as such paths simply follow a Crd isopleth for any equilibria involving cordierite. Those workers suggested several approaches to avoid this problem. The majority of these approaches were discussed in the previous section of this paper and used in our study. Our previous studies (Perchuk *et al.*, 1985, 1989, 1996, 2000; Smit *et al.*, 2001) have shown not only that the linear trajectories often cross a Crd isopleth, but

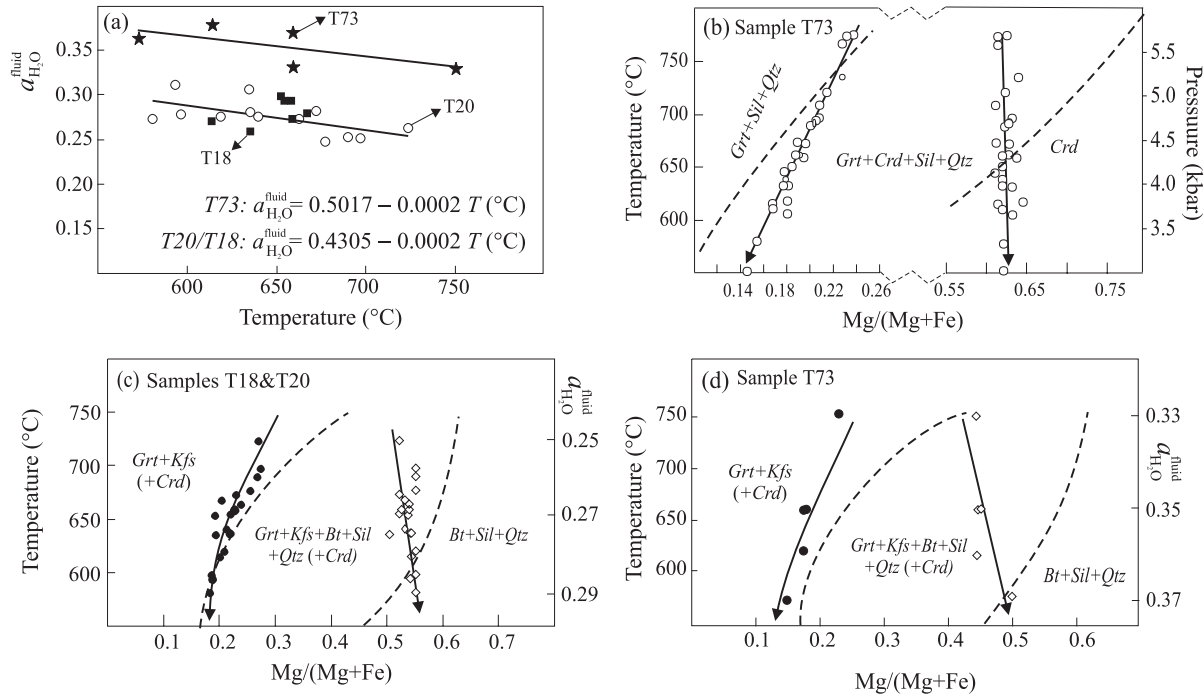


**Fig. 12.** Empirical correlations between temperature and  $a_{\text{H}_2\text{O}}^{\text{fluid}}$  (a) and phase diagrams for the mineral equilibria  $\text{Crd} = \text{Grt} + \text{Sil}_2 + \text{Qtz}$  (b), and  $\text{Fsp} + \text{Grt} + \text{H}_2\text{O} = \text{Bt} + \text{Sil}_2 + \text{Qtz}$  (c, d) in the samples T18, T20 and T73. (a) is a graphic representation of equations (20) and (21) used for calculating the phase diagrams in (c) and (d). (b) is a pseudo-projection illustrating significant changes in the Mg-number of garnet at an almost constant composition of cordierite (data are taken from Table 4), which is in accordance with the theoretical analysis done in the text. It should be noted that the arrow for the Crd composition in the diagram intersects the phase boundary in the  $T$ - $N_{\text{Mg}}$  section of Fig. 8. The phase diagrams (c, d) are projections that show a negative correlation between  $T$  and  $N_{\text{Mg}}^{\text{Bt}}$  reflecting the shift of both reactions (2) and (4) to the right side. The correlative arrows in the combined projections of (c) and (d) show a negative slope in comparison with the phase boundary in the empirical  $T$ - $N_{\text{Mg}}$  pseudosection of Fig. 11a. This reflects a crucial influence of temperature on both the Bt–Grt exchange reaction (4) and the  $\text{Grt} + \text{Kfs} \rightarrow \text{Bt} + \text{Sil} + \text{Qtz}$  net-transfer reaction (2) in the metapelites from the Baklykraal cross fold. Analytical data are given in Tables 3 and A2.

also that in many cases a linear  $P$ - $T$  path can reflect an inflection caused by a change in the exhumation process (e.g. Smit *et al.*, 2001). In the majority of cases this inflection is recorded in the formation of a new reaction texture (e.g. the intergrowth of  $\text{Grt} + \text{Sil} + \text{Qtz}$  after  $\text{Crd}$ , or the formation of  $\text{Grt} + \text{Qtz}$  symplectites after  $\text{Crd} + \text{Opx}$ ) reflecting isobaric or sub-isobaric cooling of the metapelite. In addition, in our numerical modelling of  $P$ - $T$  paths for high-grade terrains (Gerya *et al.*, 2000, 2002) we reproduced the linear or near-linear shapes of such paths reflecting synchronous changes in the rheological properties (viscosity and density) of a metamorphic rock during its decompression and cooling (i.e. exhumation). However, a theoretical argument for the linearity of a  $P$ - $T$  path has never been presented before.

As mentioned above, reactions (1)–(4) suggest a coherent change in compositions of all coexisting minerals, particularly Fe–Mg minerals, with variation of external thermodynamic parameters, i.e.  $P$ ,  $T$ , and  $a_{\text{H}_2\text{O}}^{\text{fluid}}$ . If this coherency exists, the shift of these parameters of reactions (1) and (3) is recorded by the mineral equilibria. The compositional behaviour of minerals from all simultaneously operating reactions (1)–(4) with

changing  $P$ - $T$  conditions can also be predicted from the theory of phase correspondence (Perchuk, 1969, 1977). For example, a fall in temperature leads to the redistribution of Mg from  $\text{H}_2\text{O}$ -free minerals to  $\text{H}_2\text{O}$ -bearing coexisting minerals, whereas Fe shows the reverse redistribution (Perchuk & Ryabchikov, 1976), indicating that the exchange reaction (3) should be displaced to the right side with falling temperature. With reference to the metapelites from the Baklykraal cross fold this effect is exemplified by the profiles in Figs 3d–f, 5d and 6a. At isothermal conditions the net-transfer reaction (1), i.e. the divariant equilibrium, is displaced towards Fe-rich compositions (Fig. 8) with a decreasing pressure, therefore smoothing the effect of  $T$  on the exchange equilibrium (3). However, at a constant  $P$  the temperature effect on the coherent reaction (3) is shown in displacement of the phase boundaries on the  $P$ - $N_{\text{Mg}}$  plane to the Mg-side (see Fig. 8). Thus, pressure and temperature affect the exchange reaction (3) in opposite ways. As a result, the synchronous fall of  $T$  and decrease of  $P$  must ultimately produce a negligible change in the composition of the cordierite (Table 4, Fig. 10). Thus, the linearity of a  $P$ - $T$  trajectory is the direct result

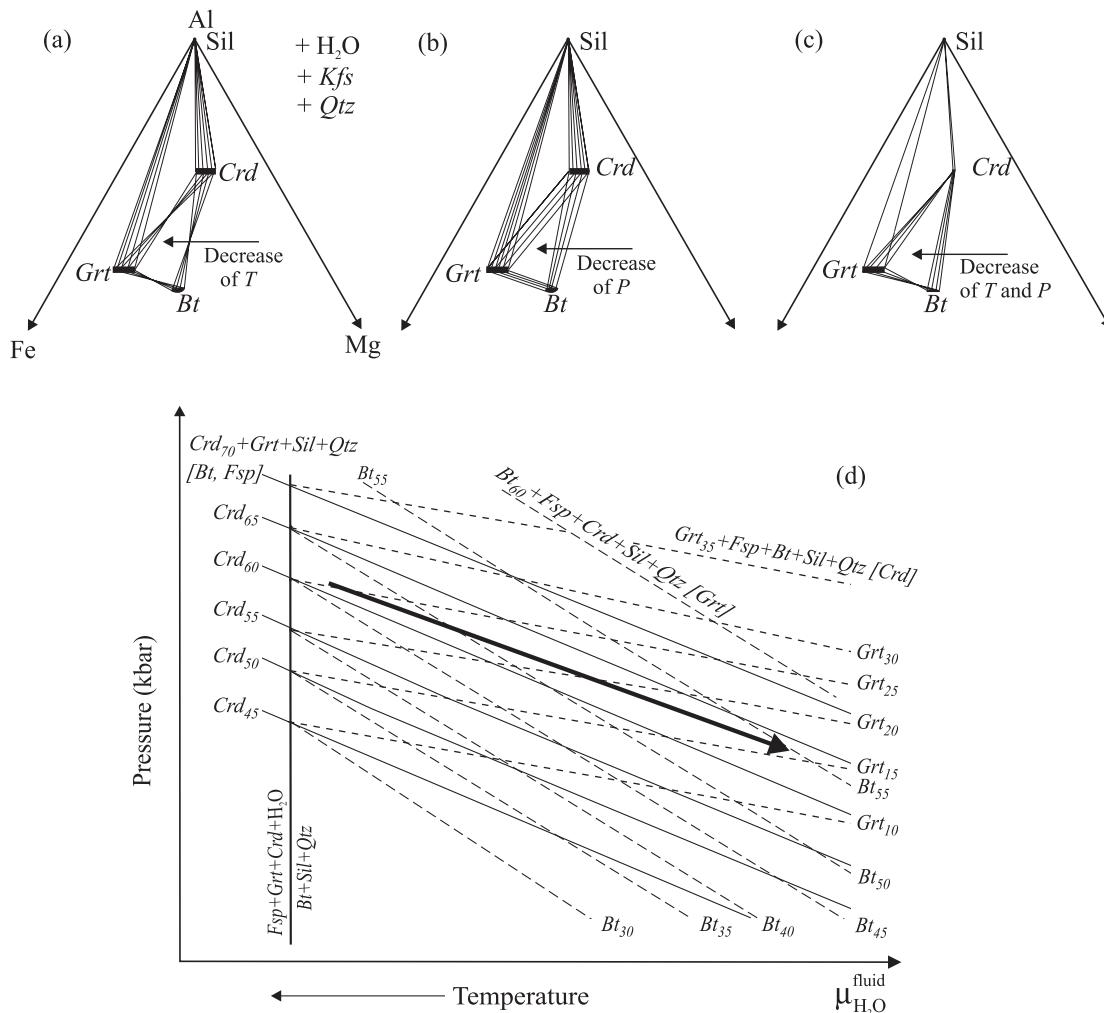


**Fig. 13.** Compositional relationships of minerals from the system KFMASH related to the  $P$ - $T$  trajectory in Fig. 10. The Kozhinskii AFM diagrams (a–c) schematically illustrate the influence of  $T$  on both the Fe–Mg exchange equilibria (Bt–Grt and Crd–Grt) at a fixed  $P$  (a), and the systematic shift of both net-transfer reactions (1) and (2) with decrease of  $P$  at constant  $T$  (b) as a part of the provisional univariant equilibrium  $\text{Crd} + \text{Grt} + \text{Fsp} + \text{H}_2\text{O} = \text{Bt} + \text{Qtz} + \text{Al}_2\text{SiO}_5$ . The synchronous decrease of  $P$  and fall in  $T$  (c) results in a negligible increase in  $N_{\text{Mg}}^{\text{Crd}}$  and a perceptible increase of  $N_{\text{Mg}}^{\text{Bt}}$ . This is clearly seen in the qualitative  $\mu_{\text{H}_2\text{O}}^{\text{fluid}}(T)$ - $P$  diagram (d) constructed by using the Marakushev approach (Marakushev & Perchuk, 1966). It should be noted that the  $P$ - $T$  path in (d) intersects isopleths of biotite in the direction of increasing Mg (in accordance with the empirical data of Fig. 9b and c). (d) shows isopleths reflecting systematic changes of Grt, Crd, and Bt in the course of the corresponding divariant net-transfer reactions (in terms of  $N_{\text{Mg}}$ ) at arbitrary and constant other compositional parameters. The isopleth related to reaction (1) is singular (line [Bt, Fsp]), whereas the other ones relate to reaction (2), [Crd]. The [Grt] isopleth reflects the reaction  $\text{Crd} + \text{Fsp} + \text{H}_2\text{O} = \text{Bt} + \text{Sil} + \text{Qtz}$ . Isopleths [Qtz] and [Sil] are not valid because no Qtz- and Sil-free metapelites occur in the studied area.

of the opposing influence respectively of  $P$  and  $T$  on the simultaneously operating reactions (1) and (3), respectively (Fig. 8).

(2) *Direction of the P–T path as a reflection of exhumation.* The decompression-cooling  $P$ - $T$  trajectory derived in Fig. 10 reflects the exhumation of the studied rocks from the middle portion of the crust to the level of about 9–10 km, where the Baklykraal cross fold was emplaced. This DC path is in agreement with our previous results on both the CZ and the SMZ of the Limpopo Complex (Perchuk *et al.*, 1996, 2000; Smit *et al.*, 2001) but differs

from published ITD paths (Horrocks, 1983; Harris & Holland, 1984; Droop, 1989; Van Reenen *et al.*, 1990; Hisada & Miyano, 1996) for other parts of the CZ.

The accuracy of the trajectory of the DC path in Fig. 10 can also be proved based on the independent biotite–garnet equilibria (2) and (4). Both divariant equilibria are independent, as neither has been directly involved in the calculation of  $P$ - $T$  paths in Fig. 9: we used reaction (2) to calculate the  $\text{H}_2\text{O}$  activity so as to correctly position Crd–Grt isopleths and for individual  $P$ - $T$  estimates. However, being part of the univariant equilibrium

Table 5: Average compositions of Fe–Mg minerals used for isopleth calculations

	Biotite	Garnet	Cordierite
Si	2.65	2.97	4.98
Ti	0.19	0.00	0.00
Al	1.74	2.01	4.01
Fe	$n$	$m$	$k$
Mg	$4.23 - n$	$2.82 - m$	$2.01 - k$
Mn	0.005	0.04	0.01
Ca	0.01	0.17	0.0
Na	0.035	0.0	0.0
K	0.90	0.0	0.0
No. of oxygens	11	12	18

$\text{Grt} + \text{Crd} + \text{Fsp} + \text{H}_2\text{O} = \text{Sil} + \text{Qtz} + \text{Bi}$ , and thus operating simultaneously with reactions (1) and (3), reactions (2) and (4) can serve as good indicators of the accuracy of the  $P$ – $T$  path derived in Fig. 10. We can prove this statement by using calculated Bt isopleths for reaction (2) as a control of the direction of the  $P$ – $T$  path of Fig. 10.

The compositional relationships of minerals for the Bt-bearing system, i.e. reactions (2) and (4), should be similar to those of the Crd–Grt equilibrium, but with one very important difference: temperature affects reactions (2) and (4) more strongly than reaction (1). Therefore, a fall in  $T$  should result in a spectrum of iron-rich coexisting biotites and garnets. At a constant pressure, this conclusion is correct and supported by a large statistical dataset (e.g. Perchuk, 1977; Perchuk & Lavrent'eva, 1983) on compositions of coexisting biotite and garnet (more than 200 pairs) from metapelites of different metamorphic complexes around the world (see Fig. 11). Figure 11a shows a comprehensive empirical phase diagram for the KCFMASH system projected onto the  $T$ – $X_{\text{Mg}}$  plane from  $P$  and  $\text{H}_2\text{O}$ . According to the diagram both  $X_{\text{Mg}}^{\text{Bt}}$  and  $X_{\text{Mg}}^{\text{Grt}}$  decrease while temperature drops. On the other hand, the arrowed lines in Fig. 12c and d tend to intersect phase boundaries copied from Fig. 11a, demonstrating an increase of  $X_{\text{Mg}}^{\text{Bt}}$  with fall in temperature. There it appears that the two diagrams of Fig. 12c and d and Fig. 11a contradict each other. However, this is only an apparent contradiction, because Fig. 11a reflects phase relations at unknown pressure and  $\text{H}_2\text{O}$  activity. In contrast, the  $X_{\text{Mg}}^{\text{Bt}}$  paths in Fig. 12c and d resulted from the simultaneous operation of reactions (1) and (3) as is controlled by changes in both the pressure and temperature as controlled by the exhumation history, i.e. the  $P$ – $T$  trajectory in Fig. 10. The Korzhinskii AFM diagrams (Fig. 13) solve this contradiction.

Accounting for the discussed competition between exchange and net-transfer reactions, the AFM diagrams in Fig. 13a–c demonstrate the strong effect of falling temperature on exchange reactions (3) and (4), and, in addition, on the Crd–Bt exchange equilibrium (5) in Table 2. This leads to an increase of  $X_{\text{Mg}}^{\text{Bt}}$  in the univariant paragenesis  $\text{Grt} + \text{Crd} + \text{Fsp} + \text{Sil} + \text{Qtz} + \text{Bt}$ , interfering with the displacement of reaction (2) to the Fe-rich side (see Fig. 11a). The resultant effect is seen in Fig. 13c, which demonstrates an extremely small, or no change in the composition of cordierite, and an appreciable increase of  $X_{\text{Mg}}^{\text{Bt}}$ . This is in contrast to the relatively large decrease of the  $X_{\text{Mg}}^{\text{Grt}}$  (compare with Fig. 12b–d and Fig. 9). In the IBD case the  $P$ – $T$  path would intersect more and more Fe-rich biotite isopleths.

The Korzhinskii method, in general, appears to be useful for the solution of such complex problems. Marakushev & Perchuk (1966) have strengthened this method by the semi-quantitative calculations of uni- and divariant lines on the  $P$ – $T$  plane from a  $\mu_{\text{H}_2\text{O}}^{\text{fluid}}$  point within the  $P$ – $T$ – $\mu_{\text{H}_2\text{O}}^{\text{fluid}}$  space, accounting for the opposite effects of the  $\text{H}_2\text{O}$  chemical potential and temperature on a hydration–dehydration reaction. Therefore, any line in the pseudoprojection of Fig. 13 suggests a systematic and coherent change of the water fugacity with falling  $T$  at a given  $a_{\text{H}_2\text{O}}^{\text{fluid}}$ . This pseudoprojection thus demonstrates, on the one hand, an increase of  $X_{\text{Mg}}^{\text{Bt}}$  along the  $P$ – $T$  path, and on the other hand the bounding of divariant reactions (1) and (2) by the univariant equilibrium  $\text{Grt} + \text{Kfs} + \text{Crd} + \text{H}_2\text{O} = \text{Bt} + \text{Qtz} + \text{Sil}$ .

Using the standard thermodynamic data from Table 2, thermodynamics of solid solutions described by equations (5)–(19), and equations (20)–(22) for each metapelitic sample we can also calculate the quantitative Bt isopleths for the assemblage  $\text{Grt} + \text{Bt} + \text{Kfs} + \text{Qtz} + \text{Sil}$  on the  $P$ – $T$  plane. We calculated isopleths for both net-transfer reactions (1) and (2) by using average compositions (formulae) of the Fe–Mg minerals coexisting in the samples (Table 5) and bounded by the integrated  $P$ – $T$  path (Fig. 10). The calculations were carried out by varying both the  $X_{\text{Mg}}$  ( $n$ ,  $m$  and  $k$ ) and  $a_{\text{H}_2\text{O}} = -0.0002247T + 0.5017$  at constant  $X_{\text{K}}^{\text{Fsp}} = 1$  (see Table A2). The limits of  $X_{\text{Mg}}$  correspond to the Mg-numbers of Crd, Grt and Bt from the samples studied. The equation for the Gibbs potential, derived from the first principles (Gerya & Perchuk, 1997), has been used for calculating the water fugacity  $(f_{\text{H}_2\text{O}}^{\text{o}})_{T,P}$ . The results are shown in the  $P$ – $T$  diagram of Fig. 14, which is a pseudoprojection from the  $\text{H}_2\text{O}$  chemical potential ( $\mu_{\text{H}_2\text{O}}^{\text{fluid}}$ ) onto the  $P$ – $T$  plane within the  $P$ – $\mu_{\text{H}_2\text{O}}^{\text{fluid}}$ – $T$  space of the KFMASH system. The  $P$ – $T$  path, taken from Fig. 10, slightly intersects the Crd<sub>63</sub> isopleth and cross-cuts both the Grt and Bt isopleths, leaving no room for any alternative interpretation (e.g. IBD) of the decompression-cooling exhumation of rocks from the Baklykraal cross fold.

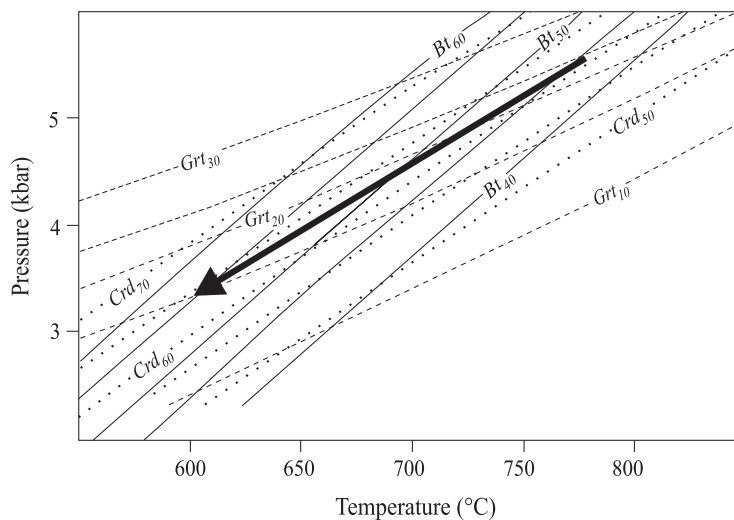


**Fig. 14.** Projection of the  $N_{Mg}$  isopleths for Bt (continuous lines), Crd (dotted lines), and Grt (dashed lines) in paragenesis with Sil, and Qtz  $\mu_{H_2O}^{fluid}$  from onto the  $P$ - $T$  plane for the KFMAS system. The isopleths for Bt in reaction (2) and Crd<sub>63</sub> in reaction (1) are calculated using the standard data from Table 2 and thermodynamics of solid solutions defined by equations (5)–(19) and projected onto the  $P$ - $T$  section from  $\mu_{H_2O}^{fluid}$ . Apart from the Mg-number, the Al content ( $X_{Al} = -0.0289X_{Mg} + 0.2581$ ) and the Ti content of biotite, other mineral chemistries correspond to average compositions of the Fe–Mg minerals from all three samples (see text). The  $a_{H_2O}^{fluid}$  varies along each isopleth according to equation (22). The arrow indicates the single integrated  $P$ - $T$  path for the metapelites from the Baklykraal cross fold (see Fig. 10). It should be noted that the integrated  $P$ - $T$  path in Fig. 10 slightly intersects the Crd<sub>63</sub> isopleth belonging to the assemblage Crd + Grt + Qtz + Al<sub>2</sub>SiO<sub>5</sub> with a negligible increase of the  $N_{Mg}^{Crd}$ . The  $N_{Mg}^{Bt}$  in the assemblage Bt + Qtz + Grt + Kfs + Al<sub>2</sub>SiO<sub>5</sub> changes more significantly along the  $P$ - $T$  path, from  $N_{Mg}^{Bt} \sim 45$  to  $N_{Mg}^{Bt} \sim 55$ . This corresponds to data from Fig. 9b and c and Tables 3 and 4. The data in this figure rule out the possibility of sub-isothermal decompression or any other possible path in a  $P$ - $T$  diagram.

## CONCLUSIONS

The Central Zone of the Limpopo Complex is characterized by the presence of two major fold types reflecting distinctly different fold geometries and intensities of deformation: (1) large steeply WSW-plunging sheath folds; (2) large NNW-SSE-trending cross folds with near-horizontal fold axis. The Avoca sheath fold and Baklykraal cross fold are respectively developed in quartzo-feldspathic gneisses (Singelele Gneiss) and rocks of the Beit Bridge Complex west of Alldays. Gneisses in the rim of the Avoca sheath fold display a strong gneissic shear fabric ( $S_2$ ) that appears to be reworked during the subsequent formation of the gneissic fabric ( $S_3$ ) that defines the form of the Baklykraal cross fold.

Structural, petrographic and mineral chemistry data for metapelitic gneisses from the Baklykraal fold reflect a distinct stage of deformation ( $D_3$ ) and mineral growth during the post-peak metamorphic evolution ( $M_3$ ) of this structure. A systematic and monotonous change of mineral compositions in retrograde reaction textures in which garnet is being replaced by the assemblage Bt + Qtz + Sil and by Crd is the only characteristic of metapelites. In addition, no polymetamorphic signatures have been observed in other rocks forming this folded structure. Using thermobarometric estimations and calculated isopleths for the corresponding divariant reactions Bt + Qtz + Sil  $\rightarrow$  Grt + Kfs + H<sub>2</sub>O and

Qtz + Sil + Grt  $\rightarrow$  Crd, belonging to the univariant equilibrium Grt + Kfs + Crd + H<sub>2</sub>O = Bt + Qtz + Sil, both the linearity and type (decompression-cooling) of a single  $P$ - $T$  path are proved. The possibility of sub-isothermal decompression is completely ruled out. These data allow only one conclusion, namely for a single decompression-cooling metamorphic ( $M_3$ ) event accompanied by a distinct deformational ( $D_3$ ) event during the emplacement of the rocks forming the Baklykraal cross fold. This ( $D_3/M_3$ ) event obliterated all petrological evidence for the early  $D_2/M_2$  event in the studied metapelitic gneisses from this major fold.

The conclusion that the  $S_2$  gneissic fabric preserved in the Avoca sheath fold was reworked during the formation of the  $S_3$  gneissic fabric of the Baklykraal cross fold is supported by recent age dating: (1) zircon SHRIMP data (Boshoff, 2004) of syn- to late tectonic precursors to the Singelele gneisses that constrain the age of formation of the Avoca sheath fold and therefore the gneissic  $S_2$  fabric to  $\sim 2.57$  Ga; (2) single-phase garnet dating from a Baklykraal metapelitic gneiss (sample T73) that clearly shows that the gneissic ( $S_3$ ) fabric of the Baklykraal cross fold developed at  $\sim 2.0$  Ga (Boshoff, 2004).

If true for the entire CZ, the results of this study provide clear evidence that closely associated sheath and cross folds record a complex poly-deformational/metamorphic history for the CZ of the Limpopo Complex.

## ACKNOWLEDGEMENTS

This work was carried out as part of the RF-RSA scientific collaboration and supported by grants from the National Research Foundation, South Africa, and the Rand Afrikaans University (to D.D.V.R.), RFBR grants 02-05-64025 (to L.L.P.) and 03-05-64633 (to T.V.G.), and the Russian State Leading Scientific Schools Program (project 1645.2003.5 to L.L.P.). Giles Droop and an anonymous reviewer are acknowledged for their detailed and very helpful reviews of the earlier version of this paper. Giles Droop also kindly reviewed the next version of the paper. We would like to thank Simon Harley for his helpful comments and for the final editing of the manuscript.

## SUPPLEMENTARY DATA

Supplementary data for this paper are available on *Journal of Petrology* online.

## REFERENCES

- Aranovich, L. Y. & Podlesskii, K. K. (1989). Geothermobarometry of high-grade metapelites: simultaneously operating reactions. In: Daly, J. S., Yardley, B. W. D. & Cliff, B. R. (eds) *Evolution of Metamorphic Belts*. Geological Society, London, Special Publications **42**, 41–65.
- Bahneman, K. P. (1972). A review of the structure, stratigraphy and the metamorphism of the basement rocks in the Messina district, Northern Transvaal. Ph.D. thesis, University of Pretoria, 156 pp.
- Barton, J. M., Holzer, L., Kamber, B., Doig, R., Kramers, J. D. & Nyfeler, D. (1994). Discrete metamorphic events in the Limpopo belt, southern Africa: implications for the application of *P-T* paths in complex metamorphic terranes. *Geology* **22**, 1035–1038.
- Boshoff, R. (2004). Formation of major fold types during distinct geological events in the Central Zone of the Limpopo Belt, South Africa: new structural, metamorphic and geochronological data. Ph.D. thesis, Rand Afrikaans University, Johannesburg, 121 pp.
- Carson, C. J., Powell, R. & Clark, G. L. (1999). Calculated mineral equilibria for eclogites in the CaO–Na<sub>2</sub>O–FeO–MgO–Al<sub>2</sub>O<sub>3</sub>–SiO<sub>2</sub>–H<sub>2</sub>O system: application to the Pouébo Terrane, Pam Peninsula, New Caledonia. *Journal of Metamorphic Geology* **17**, 9–24.
- Droop, G. T. R. (1989). Reaction history of garnet–sapphirine granulites and conditions of Archean high-pressure granulite-facies metamorphism in the Central Limpopo Mobile Belt, Zimbabwe. *Journal of Metamorphic Geology* **7**, 383–403.
- Feldtmann, F. (1996). The structural–metamorphic evolution of the marble and calc-silicate rocks of the Baklykraal quarry near Alldays, Central Zone of the Limpopo Belt, South Africa. M.Sc. thesis, Rand Afrikaans University, Johannesburg, 132 pp.
- Feldtmann, F., Smit, C. A. & Van Reenen, D. D. (1995). The significance of two major structural trends in the Central Zone of the Limpopo Belt. *Centennial Geocongress, Johannesburg, Extended Abstracts* **2**, 596–599.
- Fripp, R. E. P. (1983). The Precambrian geology of the area around the Sand River near Messina, Central Zone, Limpopo Mobile Belt. *Geological Society of South Africa, Special Publication* **8**, 89–102.
- Frost, B. R. & Chacko, T. (1989). The granulite uncertainty principle: limitations on thermobarometry in granulites. *Journal of Geology* **97**, 435–450.
- Gerya, T. V. (1991). The method of physicochemical modeling of metamorphic reactions using mass-balance equations. *Contributions to Physicochemical Petrology* **16**, 112–127 (in Russian).
- Gerya, T. V. (1999). *P-T* paths and evolution granulite facies terrains. D.Sc. dissertation, Moscow State University, 453 pp. (in Russian).
- Gerya, T. V. & Perchuk, L. L. (1994). A new thermodynamic database for thermobarometry. *International Mineralogical Association, 16th General Meeting, Abstracts, Pisa*, p. 142.
- Gerya, T. V. & Perchuk, L. L. (1997). Equations of state of compressed gases for thermodynamic databases used in petrology. *Petrology* **5**, 366–380.
- Gerya, T. V., Perchuk, L. L., Van Reenen, D. D. & Smit, C. A. (2000). Two-dimensional numerical modeling of pressure–temperature–time paths for the exhumation of some granulite facies terrains in the Precambrian. *Journal of Geodynamics* **30**, 17–35.
- Gerya, T. V., Perchuk, L. L., Maresch, W. V., Willner, A. P., Van Reenen, D. D. & Smit, C. A. (2002). Thermal regime and gravitational instability of multi-layered continental crust: implications for the buoyant exhumation of high-grade metamorphic rocks. *European Journal of Mineralogy* **14**, 687–699.
- Harley, S. L. (1989). The origins of granulites: a metamorphic perspective. *Geological Magazine* **126**, 215–247.
- Harris, N. B. W. & Holland, T. J. B. (1984). The significance of cordierite–hypersthene assemblages from the Beitbridge region of the Limpopo Belt: evidence for rapid decompression in the Archean. *American Mineralogist* **59**, 1036–1049.
- Hisada, K. & Miyano, T. (1996). Petrology and microthermometry of aluminous rocks in the Botswanan Limpopo: evidence for isothermal decompression and isobaric cooling. *Journal of Metamorphic Geology* **14**, 183–197.
- Hofmann, A., Kröner, A. & Brandl, G. (1998). Field relationships of mid- to late Archean high-grade gneisses of igneous and sedimentary parentage in the Sand River, Central Zone of the Limpopo Belt, South Africa. *South African Journal of Geology* **101**, 185–200.
- Holzer, L. (1995). The magmatic petrology of the Bulai Pluton and the tectono-metamorphic overprint at 2.0 Ga in the central zone of the Limpopo belt (Messina–Beitbridge area, southern Africa). Diploma thesis, University of Bern, 157 pp.
- Holzer, L., Frey, R., Barton, J. M., Jr & Kramers, J. D. (1998). Unravelling the record of successive high-grade events in the Central Zone of the Limpopo belt using Pb single phase dating of metamorphic minerals. *Precambrian Research* **87**, 87–115.
- Horrocks, P. C. (1983). A corundum and sapphirine paragenesis from the Limpopo Mobile Belt, southern Africa. *Journal of Metamorphic Geology* **1**, 13–23.
- Kamber, B. S., Blenkinsop, T. G., Villa, I. M. & Dahl, P. S. (1995). Proterozoic transpressive deformation in the Northern Marginal Zone, Limpopo Belt, Zimbabwe. *Journal of Geology* **103**, 493–508.
- Kreissig, K., Nägler, T. F., Kramers, J. D., Van Reenen, D. D. & Smit, C. A. (2000). An isotopic and geochemical study of the Kaapvaal craton and the Southern Marginal Zone of the Limpopo Belt: are they juxtaposed terranes? *Lithos* **50**, 1–25.
- Kreissig, K., Holzer, L., Frei, R., Villa, I. M., Kramers, J. D., Kröner, A., Smit, C. A. & Van Reenen, D. D. (2001). Geochronology of the Hout River Shear Zone and the metamorphism in the Southern Marginal Zone of the Limpopo Belt, Southern Africa. *Precambrian Research* **109**, 145–173.

- Kröner, A., Jaeckel, P., Hofmann, A., Nemchin, A. A. & Brandl, G. (1998). Field relationships and age of supracrustal Beit Bridge Complex and associated granitoid gneisses in the Central Zone of the Limpopo Belt, South Africa. *South African Journal of Geology* **101**, 201–213.
- Kröner, A., Jaeckel, P., Brandl, G., Nemchin, A. A. & Pidgeon, R. T. (1999). Single zircon ages for granitoid gneisses in the Central Zone of the Limpopo Belt, southern Africa, and geodynamic significance. *Precambrian Research* **93**, 299–337.
- Lasaga, A. C. (1983). Geospeedometry: an extension of geothermometry. *Advances in Physical Geochemistry* **3**, 81–114.
- Marakushev, A. A. & Perchuk, L. L. (1966). Physicochemical analyses of paragenesis of minerals: a review. *Geological Journal* **5**, 67–94.
- Mason, R. (1973). The Limpopo mobile belt—southern Africa. *Philosophical Transactions of the Royal Society of London, Series A* **273**, 463–485.
- McCourt, S. & Armstrong, R. A. (1998). SHRIMP U–Pb zircon geochronology of granites from the Central Zone, Limpopo Belt, southern Africa: implications for the age of the Limpopo Belt. *South African Journal of Geology* **101**, 329–338.
- McCourt, S. & Vearncombe, J. R. (1992). Shear zones of the Limpopo Belt and adjacent granitoid–greenstone terranes: implications for late Archaean collision tectonics in southern Africa. *Precambrian Research* **55**, 553–570.
- Mkweli, S., Kamber, B. & Berger, M. (1995). Westward continuation of the craton–Limpopo Belt tectonic break in Zimbabwe and new age constraints on the timing of the thrusting. *Journal of the Geological Society, London* **152**, 77–83.
- Newton, R. C. (1972). An experimental determination of the high-pressure stability limits of magnesian cordierite under wet and dry conditions. *Journal of Geology* **80**, 398–420.
- Newton, R. C. & Haselton, H. T. (1981). Thermodynamics of the garnet–plagioclase–Al<sub>2</sub>SiO<sub>5</sub>–quartz geobarometer. In: Newton, R. C., Navrotsky, A. & Wood, B. J. (eds) *Thermodynamics of Minerals and Melts. Advances in Physical Geochemistry*. New York: Springer, pp. 131–147.
- Perchuk, L. L. (1969). The effect of temperature and pressure on the equilibria of natural Fe–Mg minerals. *International Geological Review* **11**, 875–901.
- Perchuk, L. L. (1977). Thermodynamic control of metamorphic processes. In: Saxena, S. K. & Bhattacharj, S. (eds) *Energetics of Geological Processes*. New York: Springer, pp. 285–352.
- Perchuk, L. L. (1985). Metamorphic evolution of shields and fold-belts. *Geologický Zborník—Geologica Carpathica* **36**, 179–189.
- Perchuk, L. L. (1987). The course of metamorphism. *International Geology Review* **28**, 1377–1400.
- Perchuk, L. L. (1989). *P–T*–fluid regimes of metamorphism and related magmatism with specific reference to the Baikal Lake granulites. In: Daly, J. S., Yardley, B. W. D. & Cliff, B. (eds) *Evolution of Metamorphic Belts. Geological Society, London, Special Publications* **42**, 275–291.
- Perchuk, L. L. (1990). Derivation of thermodynamically consistent system of geothermometers and geobarometers for metamorphic and magmatic rocks. In: Perchuk, L. L. (ed.) *Progress in Metamorphic and Magmatic Petrology*. Cambridge: Cambridge University Press, pp. 93–112.
- Perchuk, L. L. & Lavrent'eva, I. V. (1983). Experimental investigation of exchange equilibria in the system cordierite–garnet–biotite. *Advances in Physical Geochemistry* **3**, 199–239.
- Perchuk, L. L. & Ryabchikov, I. D. (1976). *Phase Correspondence in Mineral Systems*. Moscow: Nedra, 312 pp. (in Russian).
- Perchuk, L. L., Aranovich, L. Ya., Podlesskii, K. K., Lavrent'eva, I. V., Gerasimov, V. Yu., Fed'kin, V. V., Kitsul, V. N. & Karsakov, L. P. (1985). Precambrian granulites of the Aldan shield, eastern Siberia, USSR. *Journal of Metamorphic Geology* **3**, 265–310.
- Perchuk, L. L., Gerya, T. V. & Nozhkin, A. D. (1989). Petrology and retrogression in granulites of the Kanskiy Formation, Yenisey Range, Eastern Siberia. *Journal of Metamorphic Geology* **7**, 599–617.
- Perchuk, L. L., Gerya, T. V., Van Reenen, D. D., Safonov, O. G. & Smit, C. A. (1996). The Limpopo metamorphic complex, South Africa: 2. Decompression/cooling regimes of granulites and adjusted rocks of the Kaapvaal craton. *Petrology* **4**, 571–599.
- Perchuk, L. L., Gerya, T. V., Van Reenen, D. D., Krotov, A. V., Safonov, O. G., Smit, C. A. & Shur, M. Yu. (2000). Comparative petrology and metamorphic evolution of the Limpopo (South Africa) and Lapland (Fennoscandia) high-grade terrains. *Mineralogy and Petrology* **69**, 69–107.
- Pienaar, J. C. (1985). Die Geologie van die Alldays omgewing in noord Transvaal. M.Sc. thesis, Rand Afrikaans University, Johannesburg, 158 pp.
- Pretorius, S. J. (1986). Die geologie in die omgewing van Swartwater en die Westelike deel van die Distrik Messina in die sentrale sone van die Limpopo gordel. M.Sc. thesis, Rand Afrikaans University, Johannesburg, 184 pp.
- Roering, C., Van Reenen, D. D., Smit, C. A., Barton, J. M., Jr, De Beer, J. H., De Wit, M. J., Stettler, E. H., Van Schalkwyk, J. F., Stevens, G. & Pretorius, S. (1992). Tectonic model for the evolution of the Limpopo Belt. *Precambrian Research* **55**, 539–552.
- Schaller, M., Steiner, O., Studer, I., Hozer, L., Herweg, M. & Kramers, J. D. (1999). Exhumation of Limpopo Central Zone granulites and dextral continent-scale transcurrent movement at 2.0 Ga along the Palala Shear Zone, Northern Province, South Africa. *Precambrian Research* **96**, 263–298.
- Smit, C. A. & Van Reenen, D. D. (1997). Deep crustal shear zones, high-grade tectonites and associated alteration in the Limpopo belt, South Africa: implications for deep crustal processes. *Journal of Geology* **105**, 37–57.
- Smit, C. A., Van Reenen, D. D., Gerya, T. V. & Perchuk, L. L. (2001). *P–T* conditions of decompression of the Limpopo high-grade terrain: record from shear zones. *Journal of Metamorphic Geology* **19**, 249–268.
- Söhngne, P. G. (1946). The geology of the Messina copper mines and surrounding country. *South African Geological Survey Memoirs* **40**, 280 pp.
- Spear, F. S. (1993). *Metamorphic Phase Equilibria and Pressure–Temperature–Time Paths. Mineralogical Society of America Monograph*, 799 pp.
- Spear, F. S. & Florence, F. P. (1992). Thermobarometry in granulites: pitfalls and new approaches. *Precambrian Research* **55**, 209–241.
- Spear, F. S., Kohn, M. J. & Cheney, J. T. (1999). *P–T* paths from anatectic pelites. *Contributions to Mineralogy and Petrology* **134**, 17–32.
- Tsunogai, T., Miyano, T. & Ridley, J. (1992). Metamorphic *P–T* profiles from Zimbabwe Craton to the Limpopo belt. *Precambrian Research* **55**, 259–278.
- Van Reenen, D. D. & Smit, C. A. (1996). The Limpopo metamorphic complex, South Africa: 1. Geological setting and relationships between the granulite complex and the Kaapvaal and Zimbabwe cratons. *Petrology* **4**, 562–570.
- Van Reenen, D. D., Barton, J. M., Jr, Roering, C., Smit, C. A. & Van Schalkwyk, J. F. (1987). Deep crustal response to continental collision: the Limpopo Belt of Southern Africa. *Geology* **15**, 11–14.
- Van Reenen, D. D., Roering, C., Brandl, G., Smit, C. A. & Barton, J. M. (1990). The granulite facies rocks of the Limpopo Belt, southern Africa. In: Vielzeuf, D. & Vidal, P. (eds) *Granulites and Crustal Evolution*. Dordrecht: Kluwer Academic, pp. 257–289.
- Van Reenen, D. D., Roering, D., Ashwal, L. D. & De Wit, M. J. (eds) (1992). The Archaean Limpopo granulite belt: tectonics and deep crustal processes. *Precambrian Research* **55**, 1–587.

- Watkeys, M. K. (1983). A retrospective view of Central Zone of Limpopo Belt, Zimbabwe. *Geological Society of South Africa, Special Publication* **8**, 65–80.
- Wei, C. J. J., Powell, R. & Zhang, L. F. (2003). Eclogites from the South Tianshan, NW China: petrological characteristics and calculated mineral equilibria in the  $\text{Na}_2\text{O}$ – $\text{CaO}$ – $\text{FeO}$ – $\text{MgO}$ – $\text{Al}_2\text{O}_3$ – $\text{SiO}_2$ – $\text{H}_2\text{O}$  system. *Journal of Metamorphic Geology* **21**, 163–181.
- Windley, B. F., Ackermann, D. & Herd, R. K. (1984). Sapphirine/kornerupine-bearing rocks and crustal uplift history of the Limpopo belt, South Africa. *Contributions to Mineralogy and Petrology* **86**, 342–358.
- Zyrianov, V. N., Perchuk, L. L. & Podlesskii, K. K. (1978). Nepheline–alkali feldspar equilibria: 1. Experimental data and thermodynamic calculations. *Journal of Petrology* **19**, 1–44.